University of Twente
&
Thermoplastic Composites Research Center

Reliable specific heat capacity measurements of thermoplastic composites with differential scanning calorimetry

Master thesis in Mechanical Engineering

Márton Farkas s2598272
November 30, 2023

Chair of Production Technology,
Department of Mechanical Engineering,
Faculty of Engineering Technology,
University of Twente, Enschede

Exam committee
Chair: Prof. Dr.ir. R. Akkerman
Internal supervisor: Dr.ir. M. van Drongelen
External supervisor: Ir. T. J. Asijee
External member: Dr. M. Mehrali

Summary

Carbon fiber reinforced composites have gained more attention in recent decades due to their high strength in the direction of the fiber reinforcement, along with their low density compared to metals. These properties render these materials particularly attractive to the aviation industry, where weight reduction is one of the most important goal for improving fuel efficiency and extending travel range.

Specifically, thermoplastic composites are attracting more interest due to their faster processing compared to thermoset composites, as no secondary curing step is required. Moreover, their remeltability allows them to be welded together. Consequently, various processes have been developed for these novel materials. A common feature among these processes is that they all rely on heating and cooling the material. Ultimately, the thermal properties of the composites are crucial for developing optimal process windows. Specific heat capacity is one of the necessary thermal properties and is most commonly measured by differential scanning calorimetry (DSC). However, to date, there are no well-established standards for the measurement of composites. This has led to considerable variability in the reported values for the same composite materials. Therefore, the objective of this master assignment is to investigate the existing methods and propose guidelines for reliable specific heat capacity measurements for thermoplastic composites.

Firstly, the working principle of the DSC and its application in measuring specific heat capacity is discussed. It is followed by a comprehensive literature review, encompassing previous attempts to measure the specific heat capacity of composites and also including recommendations from the DSC manufacturer. Ultimately, specific heat capacity measurements were carried out with carbon fiber reinforced polyether-ether-ketone (CF/PEEK) composites, neat PEEK, and dry carbon fibers. The choice to test neat PEEK and dry fibers was done, to test the validity of obtaining the composite specific heat capacity by the rule of mixtures.

The influence of sample mass, shape and form were investigated. Moreover, the impact of thermal cycles on the specific heat capacity were also explored. Additionally, various heating rates were tested to evaluate their influence and to gain information about the thermal gradient accumulation within the samples.

The importance of frequent baseline measurements was highlighted, as it can have a strong influence on the results. It was concluded that a sample mass of at least 15 mg is needed to minimize susceptibility to baseline deviations and achieve results with low variability. The recommendations included the use of disk-shaped specimens, in order to ensure good thermal contact between the samples and the crucibles. Heating rates between 10 and 5 K/min were advised to avoid significant temperature gradient accumulation within the samples. Employing two thermal cycles were recommended in order to erase the thermal history of the samples and to introduce one which is the same for all specimens, allowing meaningful comparisons. The careful selection of the maximum applied temperature, considering the material-dependent thermal degradation, was also emphasized.

Acknowledgments

I had a nine month long thesis project at the Thermoplastic Composites Research Center in Enschede, the Netherlands. These nine months have helped me tremendously to build a solid background for my future research and pursue engineering at the master's level. It would be unfair if I did not acknowledge all the people who have helped me through this process.

Firstly, I would like to thank my university supervisor, Martin van Drongelen, for always being available when I had questions and for providing valuable ideas and insights during my progress. I really appreciate your help. Also, thank you very much for making the administrative process of my master's thesis seamless and arranging many things for me.

Secondly, I would like to extend my gratitude, equally, to both my company supervisors, Yannick Buser and Tom Asijee. You have helped me many times in tackling the problems I encountered during my thesis. Thank you for always being available for help, not just strictly for the thesis but also for a couple of encouraging words when I was a bit overwhelmed with the work. I appreciate that during the meetings, you always took the time to go through things that bothered me, even if they were trivial or had come up multiple times. I really appreciate your help and patience with me throughout these nine months.

Special thanks to the people at TPRC for helping me in many cases and making my time there fun. Special thanks also go to the people at the University of Twente. Thank you, Nick Helthuis, for showing me how to operate the DSC machine and answering all my silly questions during my time there.

Lastly, I would like to thank my family for giving me the opportunity to complete my master's studies in the Netherlands and for always supporting me throughout the whole process. It really means a lot. This would not have happened if it weren't for you.

Contents

1 Introduction

The use of fiber reinforced composites started to emerge in 1960s, as they allowed for the development of lightweight components without compromising on strength. Various industries, including the aerospace and automotive, have adopted these novel materials. Moreover, they are commonly utilized in civil structures such as the blades of the wind turbines, as well as in high-performance sports equipment including tennis rackets and skateboards. [1] [2]

The two main constituents of the composite materials are the matrix and the reinforcement. The reinforcement provides the strength and stiffness to the composite part, while the matrix phase binds the reinforcements together and protects them from the environment. There are various types of matrix materials available such as metals, ceramics and, most commonly, polymers. In terms of reinforcements, carbon, glass and aramid fibers are frequently used. They can be in the form of particles, short chopped fibers, or long continuous fibers.[3]

1.1 Fiber reinforced polymer composites

Fiber reinforced plastics have excellent strength to weight ratio and high specific strength, as well as, good fatigue resistance compared to their metallic counterparts.[4] [3] Carbon fiber-reinforced plastics are generally considered chemically inert materials with high damping properties, although their chemical resistance may vary depending on the polymer matrix used. Given these properties, they have become very attractive materials for the aviation sector, where weight reduction is one of the primary goals. Lower weight increases the fuel efficiency, allowing the aircraft to fly longer distances with the same amount of fuel. Moreover, the increased fuel efficiency reduces the carbon footprint of the flights paving the way towards better sustainability. As an example, the Boeing 787 Dreamliner incorporates numerous composite parts in its design, amounting up to 50 [%] of the total weight of the aircraft, as illustrated in Figure 1. The primary weight bearing structures, such as the fuselage and the wings, as well as the vertical and horizontal stabilizers, predominantly utilize composite materials, leading to a lightweight and fuel efficient airliner.[5] Moreover, the better fatigue resistance of the composite fuselage allowed the manufacturer to incorporate larger sized windows compared to previous models, enhancing the passenger experience.[6] It is worth noting, that most of the composites employed in the aircraft feature a thermoset polymer as matrix material. Manufacturing of thermoset composites generally takes more time, than of the thermoplastics, due to the necessary curing step after consolidation, which hinders the further reduction of cycle times and automation. Furthermore, once the thermoset composites have solidified, they cannot be remelted, ruling out the possibility of welding and posing challenges for end-of-life recycling, as the recycling processes lead to inferior material properties than of the original parts. [7] [8]

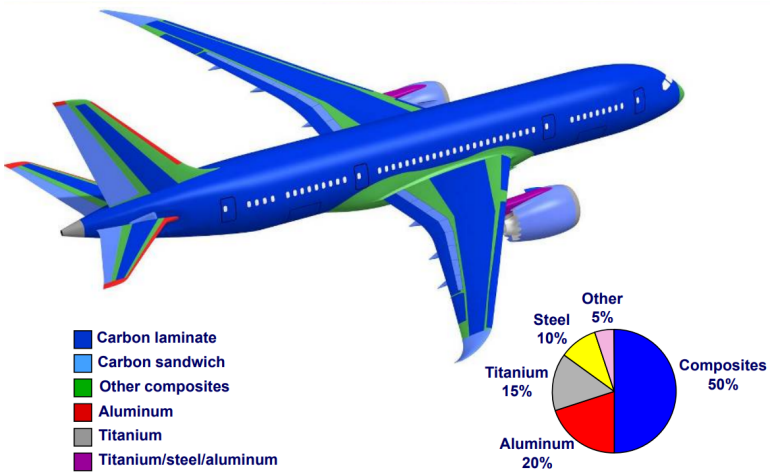

Figure 1: Material composition of the Boeing 787 Dreamliner [9]

1.2 Processing of thermoplastic composites

Thermoplastic composites (TPCs) have gained more and more attention in the last 25 years, with the aim of further improving upon the production times and reducing weight.[10] They can be processed faster than their thermoset counterparts, since there is no need for a secondary curing step. As a result, various processing technologies have been developed for thermoplastic composites, often in conjunction with each other. These methods include, but are not limited to, stamp forming, injection molding or tape placement. All these processes involve subjecting the composite part to elevated temperatures in order to facilitate polymer chain mobility. Subsequently, with the application of pressure, the part is shaped into to the desired configuration and finally cooled down to achieve final solidification.

In the case of stamp forming or thermoforming, the composite part is heated above the melting temperature of the polymer matrix, then it is placed between two pre-heated dies to be pressed into the desired shape. When cooled down the resultant part is removed from the mould.[11]

During injection molding, the molten thermoplastic resin is mixed with short fibers, then injected into a mold under high pressure to form the final product. The high pressure is maintained throughout the process to inject additional molten material in order to account for the shrinkage of the thermoplastic resin upon cooling.[12]

Thermoplastic composites can also be processed with tape placement. In this novel fabrication technique, composite tapes are laid down in a predetermined pattern onto a previously consolidated composite laminate under locally applied heat and pressure. This process results in a part with the desired thickness and reinforced in the targeted orientations. [13]

Furthermore, thermoplastic composites can be repeatedly softened by increasing the temperature and hardened by decreasing the temperature. As a result, their weldability can prevent the use of metal fasteners and adhesives. These factors contribute to the production of generally lighter and stronger parts, as they erase metal fasteners and fastening holes, thereby reducing weight and minimizing the stress concentration points.

Last but not least, welding allows for a higher degree of automation, which can further decrease the manufacturing time and drives the assembly the costs down. [8] [14] There are various welding technologies available which include, but not limited to, vibration, rotational, heated tool, resistance and induction welding.[15] These welding techniques mainly differ in how the heat and pressure is applied to the welding zone.

1.3 Importance of the specific heat capacity in the processing of TPCs

An essential feature that all the above-mentioned manufacturing processes and welding techniques share is that they all rely on heating and then cooling the material. Unsurprisingly, the thermal properties of TPCs are of great importance for developing optimal process windows for these production techniques. With the aim of eliminating, or at least, minimizing the cumbersome and expensive trial and error approach, as well as to reduce waste and save time. One of the thermal properties, specific heat, plays an important role in determining the heating response of the composite materials. By definition, specific heat capacity of the materials expresses the quantity of energy needed to raise one unit mass of the material by one unit temperature. [16] The following paragraphs highlight the significance of this material property in the processing of thermoplastic composites.

In the case of thermoforming, it still remains challenging to accurately determine the temperature profile of the composite laminates in the heating step. During this step the composite material is heated above its melting temperature and then placed between the two preheated dies to be pressed into the desired shape. Optimizing the heating step can improve the process efficiency, since it has been the primary constraint with regards to cycle time. Moreover, this step also predetermines the formability of the composite part when placed into the mold.[17] Manuel Langauer et al.[17] noted, that satisfactory modelling of the heating response can only be achieved, when taking into account the anisotropic nature of the thermal conductivity and the thermal expansion coefficient, as well as using the temperature dependent specific heat capacity of the tested material. They highlighted the importance of measuring the specific heat capacity over the interested temperature range instead of assuming a constant value, since it has allowed them to accurately follow the experimental heating curve with their simulations.

Precise control of the temperature profile of the composite tapes in automated tape placement or fiber placement is crucial in order obtain high quality bonds between the layers, resulting in composite parts that are suitable for automotive and aviation applications. Yassin et. al.[10] have reviewed various papers concerning the processing of thermoplastic composites via automated fiber placement and tape laying methods. Most of the developed simulation models used the two dimensional heat transfer equation to predict the temperate profile in the laminate during processing, shown in Equation 1.

$$k_L \frac{\partial^2 T}{\partial^2 x^2} + k_T \frac{\partial^2 T}{\partial^2 y^2} + \rho m_m H_f V \frac{\partial c_m}{\partial x} = \rho C_p V \frac{\partial T}{\partial x}, \tag{1}$$

where T is the temperature, k_L is the longitudinal thermal conductivity, k_T is the transverse thermal conductivity, ρ is the density, m_m is the mass fraction of the thermoplastic matrix, H_f is the heat of crystallization, V is the line speed, c_m is the crystalline fraction the polymer matrix, C_p is the heat capacity. Amongst others, the governing equation relies on three intrinsic thermal properties of the material, namely the specific heat capacity, the longitudinal and transverse thermal conductivity. Specific heat capacity determines the amount of energy required to input in order to heat up the composite material to its optimal processing temperature. Consequently, obtaining accurate values of these material properties are crucial for precise process simulation and control.

Regarding the welding technologies of TPCs, the temperature of the heat affected zone during welding greatly influences the quality of the resultant bond. The temperature must be high enough to facilitate the molecular diffusion at the weld interface to create the bond, but avoiding deconsolidation. According to Reis et. al. [18] composites with amorphous polymer matrix should not be heated above 75 [%] of their glass transition temperature, as for composites with semi crystalline polymer matrix the maximum temperature should not exceed 75 [%] of the polymer melting temperature. This finding shows the importance of knowing the temperature profile and precisely controlling it during welding. In order to do that, one must model the heat transfer of the welding process described by the general heat equation. This is generally done by one of the commercially available finite element method (FEM) software. The material properties necessary to solve this equation are the thermal conductivities of the composite material in the three principal directions (x,y,z), the density and the specific heat capacity of the composite material.

To conclude the thermal properties of the composite materials play a vital role in accurate process control and simulation. Knowing the required energy input for heating up or cooling down the materials are strongly dependent on the specific heat capacity. Proper characterization and consideration of this property enable precise temperature control, optimized heat input, balanced cooling rates, and ultimately, the production of high-quality products with desirable mechanical properties.

1.4 Problem statement

Even though specific heat capacity is a common material property and crucial for process simulation as detailed above, it still remains challenging and tedious to accurately and reliably measure this material property with processes and standards developed for pure polymers and other types of materials. In contrast to the mechanical characterization of the composites, which have been extensively covered by the ASTM standards, standardized test methods for thermal characterization is still yet to be developed. Therefore, several authors have obtained the specific heat capacity values of their heterogeneous composites materials by the rule of mixtures (ROM).[19] [20] [21] [22] Using the ROM, the specific heat capacity of the composite material is obtained, as the weighted average of the individual constituents. [23] However, various assumptions must be true in order to result in an accurate prediction. Such as the homogenity of the composite, which assumes that the constituents are uniformly distributed throughout the material.[24] Moreover, in most cases where the authors used the rule of mixtures,

they neglected the temperature dependency of the specific heat capacity. To date, there is a lack of literature evaluating the accuracy and applicability of the rule of mixture for calculating the specific heat capacity of composites.

Differential scanning calorimetry (DSC), detailed in subsection 2.1, is the most widely used technique for characterizing the specific heat capacity of an unknown substance, due to its ease and relative speed compared to other techniques such as adiabatic calorimetry.[25] However, a substantial problem for composite materials still persists. There are no clear guidelines regarding sample preparation and measurement conditions, including the heating rate and temperature program, which poses considerable challenges in accurately characterizing the specific heat capacity of these materials. In the following paragraphs several studies will be elaborated to showcase the difficulties of obtaining this material property and to highlight the considerable variability in the reported values for the same type of composite materials.

Sambasivam [26] measured the specific heat capacity of unidirectional epoxy based glass fiber composites with 57 % fiber volume fraction. He has tested 4 samples with similar masses of around 10 mg, using 5 K/min heating rate following the ISO 11357-4 standard. His results have shown significant variability between the measured specific heat capacity values, despite having the same material, temperature program and heating rate, depicted on Figure 2. The author has not given a direct explanation on the cause of this material inconsistency. However, he mentioned, that the fiber volume fraction can slightly vary across the laminate, resulting in polymer rich or fiber rich regions, which is not taken into account in the specific heat capacity calculation.

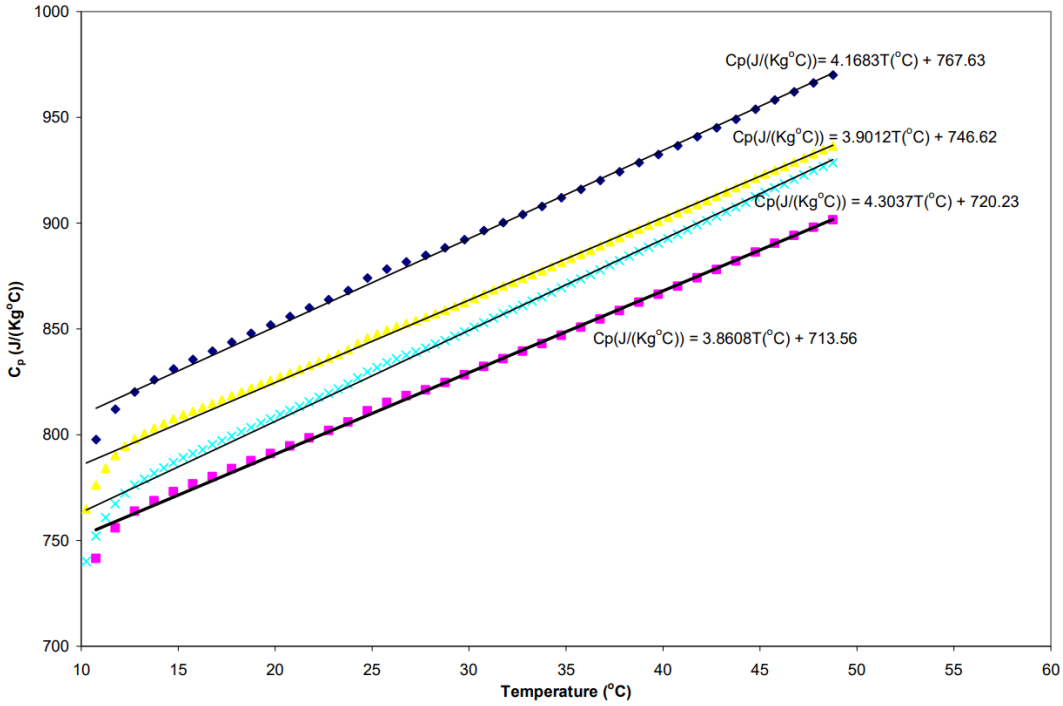

Figure 2: Variability of the specific heat capacity values of unidirectional glass-fiber/epoxy composite [26]

Garcia [27] has measured the specific heat capacity of carbon fiber reinforced polyimide composites over a wide range of temperatures. His results have shown the significant influence of the measurement parameters, such as the heating rate on the resultant specific heat capacity. By varying the heating rate between 5 K/min and 30 K/min notable discrepancies were observed in the obtained specific heat capacities even at lower temperatures, which further emphasises the need for standardized measurement conditions.

In the case of carbon fiber reinforced polyetheretherketone (CF/PEEK) composites, a broad scatter of the reported specific heat capacity values can be observed, when comparing the available data from the open literature, even though the material composition and the fiber volume fraction were the same in all cases. Table 1 shows several papers where this material property was found. It should be noted, that the papers listed in the first three rows of Table 1 reported temperature independent specific heats. Additionally, the exact temperature at which these values were calculated was not specified in their work, hindering their comparability. Several authors obtained this material property by using the rule of mixtures due to its ease compared to DSC or flash DSC measurement, but no evaluation was found regrading the reliability of this approach. From row 4 to 7, the listed papers included temperature dependent specific heats. The results from Cogswell[28] and Dennis et al.[29] at room temperature show a good match, in contrast to the specific heat from Omar et al.[30], that is more than 200 J/kgK higher. At 300 °C a much more notable difference can be observed between values from Cogswell [28] and Dennis et al.[29], no data was available in the work of Omar et al.[30] at this temperature. Surprisingly, at 400 °C Omar et al.[30] reports almost the same value as Cogswell[28], despite the notable difference at room temperature. Zhao et al.[31] also reported temperature depended specific heat capacity values, although the source was not referenced. However the results perfectly coincide with Cogswell [28], therefore it is highly probable, that Cogswell [28] was the root source.

Table 1: Specific heat capacity values of CF/PEEK found in the literature

Ref.	**Material**	**Specific heat capacity [J/kgK]**	**Temp.[°C]**	**Cp calculation**
[32]	CF/PEEK	1425	Temp. independent	Rule of mixtures
[22]	CF/PEEK	1700	Temp. independent	Rule of mixtures
[33]	CF/PEEK	1370	Temp. independent	Rule of mixtures
[30]	CF/PEEK	1100 - 1800	25 - 400	Not specified
[28]	CF/PEEK	865 - 1550 - 1700	25 - 300 - 400	DSC
[31]	CF/PEEK	865 - 1550 - 1700	25 - 300 - 400	Not specified
[29]	CF/PEEK	886 - 1803	25 - 300	Flash DSC

To conclude, the lack of standardization leads to inconsistencies and discrepancies in reported results across different studies, hindering the comparability and reliability of the data. Such standardization efforts will not only enhance the accuracy and reliability of specific heat capacity measurements, but will also allow meaningful comparisons between different studies to further promote the advancements in the field. A comprehensive overview of the previous attempts for characterizing the specific heat capacity of composites by differential scanning calorimetry can be found in subsection 3.1.

1.5 Research objective

Based on the challenges elaborated in the problem statement, the research objective of this graduation assignment is to analyze the existing specific heat capacity measurement methods by the means of DSC and to investigate and understand the influence of measurement parameters as well as the effects of sample types and preparations. This is done, for the purpose of formulating guidelines and recommendations for accurate and reliable specific heat capacity measurements for thermoplastic composites.
In order to fully address the research objective three sub questions were formulated, which are listed below:

1.1 How does the sample preparation influence the specific heat capacity measurement and what is the desired sample preparation for reliable and consistent specific heat capacity measurements for TPCs in terms of sample weight, form and shape?

1.2 How do the operating conditions influence the specific heat capacity measurements and what are the recommended testing parameters for reliable and consistent specific heat capacity measurements?

1.3 Does a thermal gradient occur within the samples upon the DSC measurements, and if so how influential it is on the resultant specific heat capacities?

1.6 Approach

In section 1 the importance of obtaining precise heat capacity values for thermoplastic composites is highlighted along with the challenges associated with such task. In section 2 the working principle of the differential scanning calorimetry is discussed, the primary technique used for measuring specific heat capacity of an unknown substance. This chapter concludes with a detailed explanation of currently available standards for specific heat capacity determination with DSC instruments. In section 3 a comprehensive overview of the corresponding literature on characterizing the specific heat capacity of composites is provided. Additionally, the guidelines and recommendations from the DSC machine manufacturer for accurate heat capacity measurements were detailed here. In section 4 the tested materials, their essential properties, and the manufacturing process employed for sample production is discussed. This chapter also covers sample preparations, the varied measurement conditions, and the experimental procedure. In section 5 the results of the measurements are presented, followed by a detailed discussion in section 6. The proposed guidelines and best practices for heat capacity determination for thermoplastic composites are presented at the end of section 6. In section 7, the conclusion and the recommendations for future work are outlined. Figure 3 shows the schematic of the approach that was followed in this study.

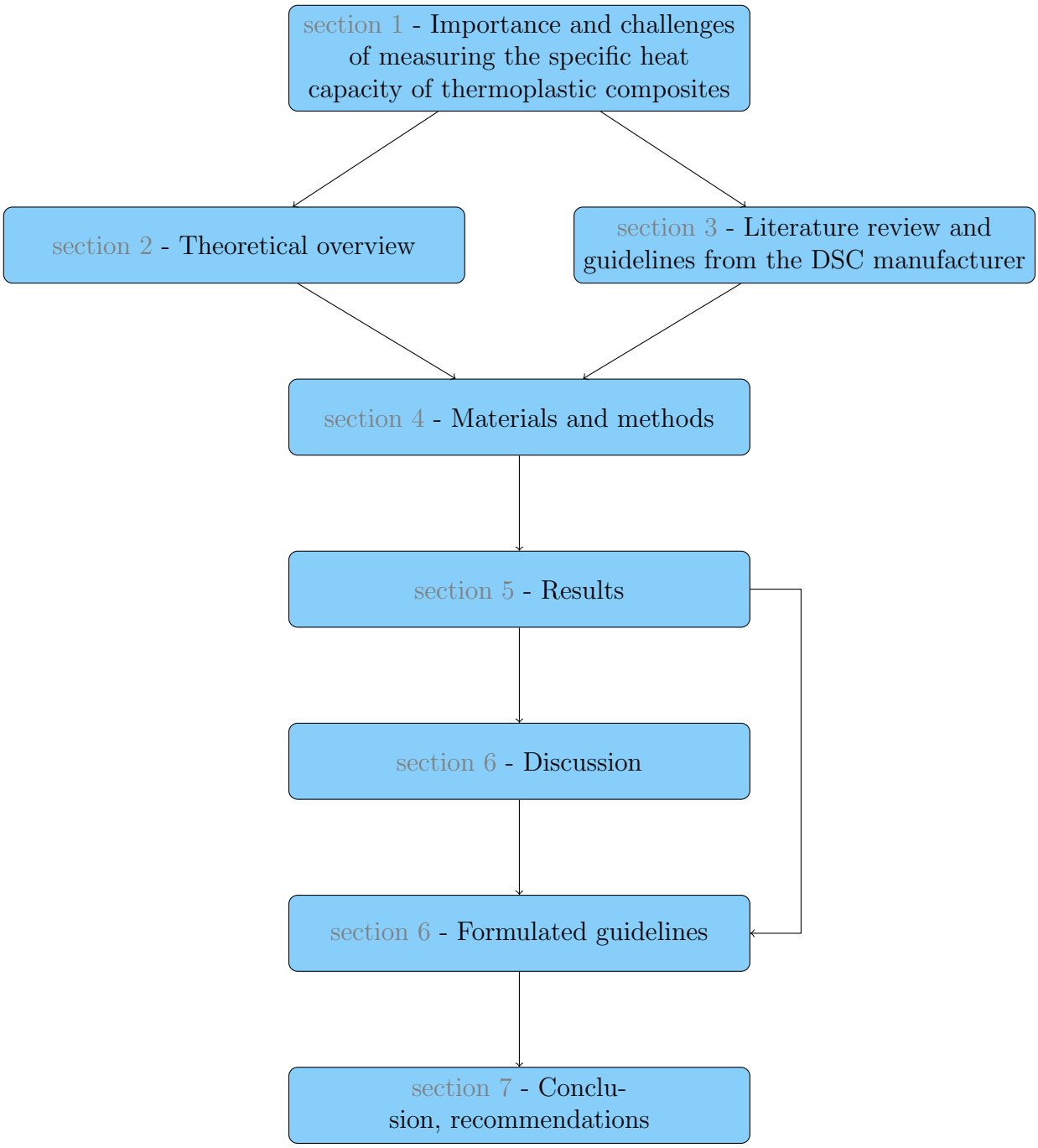

Figure 3: Schematic of the approach

2 Theoretical background

In this section the working principle of the differential scanning calorimetry will be elaborated as this technique was used in this study to measure the specific heat capacity of the composite samples. This is followed by describing the necessary working equations and theory for heat capacity determination by DSC, according to the ASTM standard.[34]

2.1 Differential scanning calorimetry

Caloric measurements have been carried out for centuries with the main objective of quantifying the heat transferred to or from a substance. The precise measurement of heat flows can help to better understand the associated physical and chemical transitions taking place in the materials when heated up or cooled down. Moreover, it serves as a powerful tool for characterizing the thermal properties of a wide range of materials. Joseph Black, a university professor in the 18th century at the University of Glasgow, laid down the foundations of calorimetry with his groundbreaking work on latent heat. [35] Numerous calorimeter designs, including the modern differential scanning calorimeter, were developed based upon his work. [36]

In principle, differential scanning calorimetry measures the difference in the heat flow rate between the sample of interest and a reference, when both subjected to a controlled temperature program. In other words, it measures the difference in energy input into the sample and the reference as a function of temperature.[36] [37] Using the heat flow rate difference, the heat capacity of the material can be calculated across the measured temperature range amongst others. In the convectional heat flux DSC cell, shown in Figure 4a, the pans containing the sample and the reference material sit on elevated platforms on a thermoelectric disk. The thermoelectric disk serves as the primary mean of heat transport from the furnace to the sample and to the reference. The sample and reference temperature difference are measured by chromel-constatan area thermocouples welded to the underside of the elevated platforms. Since heat flow difference cannot be measured directly, the temperature difference output from the thermocuples is fed into a computer, which amplifies and scales the signal to be read directly in heat flow units. Alumel and chromel wires are also attached to the underside of the thermocouples, allowing the continuous monitoring of the sample temperature throughout the measurement. [38] In order to obtain the sample heat flow, a simple one term expression can be used, which is analogous to Ohm's law in electronics. The equation relates the temperature difference measured by the thermocouples to the heat flow in or out of the sample, shown in Equation 2.

$$Q = \Delta T / R, \tag{2}$$

where Q is the sample heat flow, ΔT is the temperature difference between the sample and reference temperature sensors, and R is the thermal resistance of the thermoelectric disk from the furnace to the sample and reference positions. Most conventional DSC

machines use this one term equation for heat flow calculation. However, it is important to note, that this simplified equation assumes that the temperature of the furnace on the sample side and on the reference side is the same. Moreover, it assumes a perfectly symmetrical DSC cell, meaning that the thermal resistance of the cell from the furnace to the sample is the same as the thermal resistance from the furnace to the reference. However, this can never be fully satisfied due to the inherent limitations in manufacturing accuracy. [39] To overcome such constraints, Ta instruments have developed a novel cell design, furnace placement and heat flow equation, which is implemented in the DSC 250 machine, available at the University of Twente laboratory. The detailed explanation of this novel Tzero cell design can be found in subsection A.1.

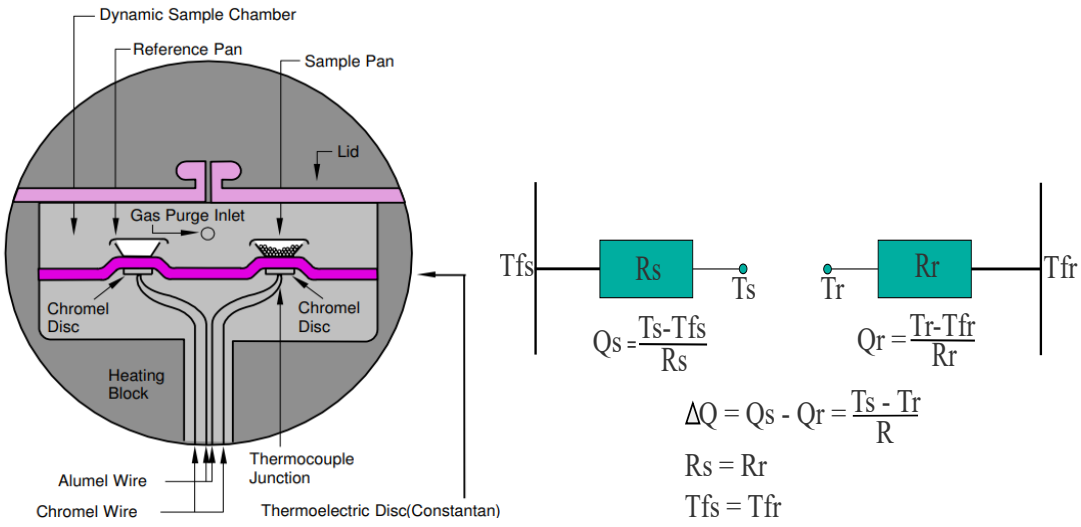

(a) Schematic of a heat-flux DSC cell [40] (b) Thermal circuit of the heat-flux DSC [41]

Figure 4: Heat-flux DSC Cell and its thermal circuit

2.2 Determination of specific heat capacity using DSC

Using differential scanning calorimtery, the specific heat capacity of the sample is proportional to its heat flow rate and can be calculated following standardized procedures described by American Society for Testing and Materials (ASTM) and by the International Organization for Standardization (ISO) as well. [34] [42] Both standards employ a comparative approach for c_p determination, in which the heat flow of a standard material, with well defined specific heat capacity, is compared to the heat flow of the sample under identical measurement conditions. The specific heat capacity of the sample is then determined from their respective heat flow ratio. This comparative technique requires three subsequent DSC runs with the same experimental program. In the subsequent sections, the ASTM E1269-11 [34] standard will be detailed, as that one was followed to obtain the specific heat capacity of the tested samples in this thesis.

First, the 'Baseline' run must be completed with two empty crucibles placed in the DSC cell. This measurement is needed to account for the inherent bias of the instrument, since most DSC machines exhibit a heat flow offset from zero even when there

is no material present in the cell. This is caused by the manufacturing inaccuracies, resulting in slightly different thermal resistances in the two sides of the cell as well as by the non-perfect adiabatic heat transfer. This measured baseline will then be used to subtract from the heat flows of the reference and sample materials. In the second run a reference material, usually synthetic sapphire (Al_2O_3), with a well defined specific heat capacity is tested, which will serve as the comparison basis for the sample heat capacity determination. Lastly, the sample with the unknown specific heat capacity is tested. [34] The results of the three subsequent dsc runs are three heat flow temperature curves as shown in Figure 5.

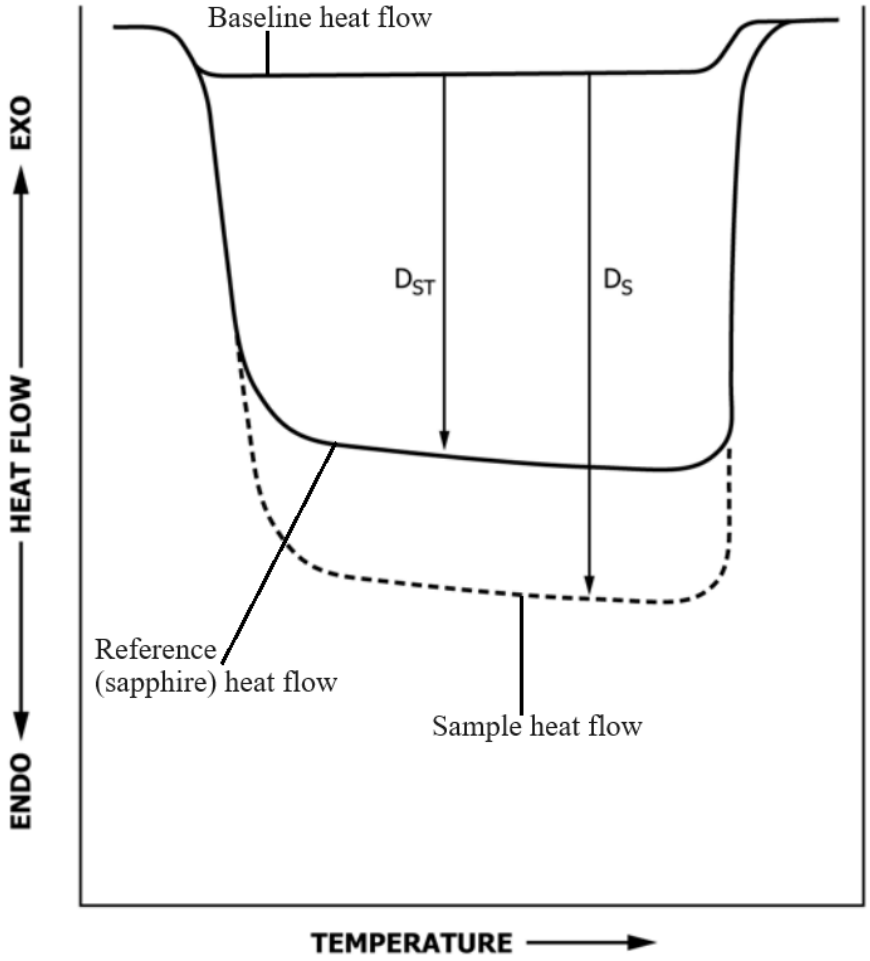

Figure 5: Baseline, sapphire, sample heat flow - temperature curves [34]

From these curves the heat flow difference between the baseline and the standard material (Dst), and the heat flow difference between the baseline and the sample (Ds) can be obtained. With the help of these two heat flow differences, the specific heat capacity of the sample can be calculated. If the baseline and reference material measurement is done prior to every sample measurement the specific heat capacity of the sample can be calculated using the expression below. [34]

$$C_p(s) = C_p(st) \cdot \frac{D_s \cdot W_{st}}{D_{st} \cdot W_s}, \tag{3}$$

where $C_p(s)$ is the specific heat capacity of the sample, $C_p(st)$ is the specific heat capacity of the sapphire standard, D_s is the heat flow difference between the baseline and the sample heat flow, D_{st} is the heat flow difference between the baseline and sapphire standard heat flow, W_{st} is the mass of the sapphire standard and W_s is the mass of the sample. If the baseline and reference runs are carried out regularly, but not prior to every sample measurement, the calorimetric sensitivity of the machine has to be obtained first. This expression, shown in Equation 4, compares the thermal mass (mass · specific heat capacity) of the reference material to its literature value, serving as a correction term.

$$E = [b/(60 \cdot D_{st})][W_{st} \cdot C_p(st) + \Delta W \cdot C_p(c)], \tag{4}$$

where b is the heating rate, ΔW is the pan mass difference between the empty pan that is replaced by the pan containing the sapphire standard , if not the same pan used for both measurements. $C_p(c)$ is the aluminium crucible specific heat capacity. With the known calorimetric sensitivity, the specific heat capacity of the unknown sample can be calculated using Equation 5. In this expression, the first term gives the specific heat capacity of the unknown sample, since in a DSC experiment the specific heat capacity can be calculated by dividing the heat flow by the heating rate times the mass of the sample. The second term compensates for the possible pan mass difference between the empty pan and the pan containing the sample.

$$C_p(s) = \frac{60 \cdot D_s}{W_s \cdot b} - \frac{\Delta W \cdot C_p(c)}{W_s} \tag{5}$$

,where ΔW is the pan mass difference between the empty pan and the pan containing the sample. Regrading the measurement conditions, the ASTM e1269 standard recommends a 4 [min] isothermal hold at the initial temperature to ensure equilibrium before the start of the experiment. As for heating rate, the standard[34] advises 20 [K/min].

3 Literature review

After exploring the corresponding literature, a few sources have been found, where the authors had attempted to measure the specific heat capacity of composites previously, summarized in Table 2. The first part of the literature review in subsection 3.1 provides a overview of these attempts, in subsection 3.2 the manufacturers recommendations have been reviewed for accurate and reliable specific heat capacity measurement with their dedicated machinery.

3.1 Literature overview of previous attempts for characterizing the specific heat capacity of composites

During the literature review, various papers were found that measured the temperature-dependent specific heat capacity of composites with both thermoset and thermoplastic matrices. In the work of Johnson [43], the thermoset matrix was epoxy, reinforced with carbon fiber. Similarly, Kaloginnakis et al. [44] prepared epoxy-based composites with carbon fiber and also with glass fiber reinforcements. Cecean et al. [45] measured aramid-reinforced composites, in addition to those with glass and carbon fibers, using both epoxy and polyester matrices. Regarding the thermoplastic composites, the reviewed papers used PEEK [46][47], PES [48], and PP [3] matrices with carbon fiber reinforcement in the first two cases and with glass fiber reinforcement in the case of PP.

Regarding the sample fabrication, Cecean et al. [45] employed the hand layup method to obtain the layered samples, while Johnson [43] tested uncured epoxy-based composite samples. Forghani [47] used the as-received tapes in his work without post-processing, whereas Kollmannsberger et al. [48] utilized layered samples processed by an AFP machine. The sample fabrication process was not detailed in the other cases [3][44]. Therefore, the measured samples had various thermal histories due to differences in their processing methods.

Heat capacity measurements were carried out using both conventional DSC [45][43] [46][3] and temperature-modulated DSC (TMDSC).[44][47][48] The TMDSC technique employs the same apparatus as conventional DSC, utilizing a linear heating ramp, but also superimposes a sinusoidal signal on this ramp [49]. The standard followed for heat capacity determination was explicitly specified only in the works of Cecean et al. [45] and Kaloginnakis et al. [44]. In the other cases, only the technique used was mentioned.

There is no uniformity in terms of sample masses across the reviewed papers, varying between 8.4 and 20 mg. It is also worth pointing out that four of the papers [43] [46][48][3] did not specify the applied sample mass. Regarding the layup orientation, both cross-ply [44] and unidirectional (UD) layups have been utilized.[45][43][47][46] In cases where the authors specified, they used disk-shaped samples [45] [44], while in other cases, no information was found about the sample shape.[43][47][46][48][3]

The majority of the authors [45][44][43, 3] tested three samples per material configuration. Kollmannsberger et. al. [48] measured 5 samples and used the average values for heat capacity determination, while two authors [47][46] did not specify the number of tested samples.

The measured temperature range varies significantly across the reviewed papers, with a minimum temperature of -50 °C in the work of Kaloginnakis et. al. [44] and a maximum tested temperature of 420 °C in the work of Kollmannsberger et. al. [48]. The applied heating rate was 10 K/min using conventional DSC, where the authors mentioned it.[45][3] However, no information was found about the applied heating rate in the works of Johnson [43] and Muhammad [46]. For TMDSC, the applied linear heating rates were either 3 K/min [47][48] or 5 K/min [44], with modulations of either 0.5 or 1 K.

Cecean et. al. [45] reported a 3.5 % uncertainty regarding his heat capacity determination. Kaloginnakis et. al. [44] reported remarkably low standard deviations of 2 % and 3 % for their epoxy/glass and epoxy/carbon fiber materials, respectively. In the work of Forghani [47], the standard deviation of the results was not specifically mentioned. However, his reported results vary between 700 J/kg·K and 1020 J/kg·K at 50 °C and 1520 J/kg·K and 1720 J/kg·K at 360 °C, showing deviations of 18 % and 6 %, respectively. In the work of Kollmannsberger et. al. [48], the error bars in the results showcase a roughly 6 % and 3 % variation at the lowest and highest temperatures, respectively. In two cases[43][3], no mention was found regarding the scatter of their results.

Last but not least, several authors [45][44] have reported the difficulty of obtaining representative samples due to the small size of the crucibles. Moreover, Cecean et. al. [45] mentioned the effort to flatten the specimens prior to the heat capacity measurement to achieve as good contact as possible between the samples and crucibles. A detailed review of the selected papers can be found in subsection A.2.

It is worth noting, that during the literature review, several papers were found, where the authors reported specific heat capacity values of CF/PEEK composites. However, it was observed that these values were not directly measured in their respective studies, but rather obtained from other sources. Figure 6 below showcases, that most of the values found in the literature reference back to only one paper. Unfortunately, that paper is unavailable, therefore it is hard to evaluate the reliability of the source. The only information that was openly available about the work Blundell et al.[50], was found in the thesis of Forghani[47]. He elaborated, that Blundell et al.[50] obtained the temperature dependent specific heat from the reported enthalpy values for CF/PEEK composite. These findings further reinforce the point, that the specific heat capacity of composites, especially in the case thermoplastic composites, has long been neglected, and only a few efforts have been made to characterize this crucial material property. [50]

To conclude, few sources have been found in the open literature, where the measurement of the specific heat capacity of the composite materials were well documented addressing the sources of errors and the uncertainty of the results. Moreover, in terms of sample preparation and sample weights there is no consensus over the reviewed papers. The same applies to the measurement conditions, including the employed employed heating rate and the temperature program.

Table 2: Summary of the reviewed papers

Ref.	Material	Temp. range [°C]	Heating rate [K/min]	Sample weight [mg]	Cp determination	Remarks
[45]	Epoxy/GF/CF/Aramid Polyester/GF/Cf/Aramid	20 - 250	10	8.4 - 17.9	DSC Three run method	UD samples made with hand-layup Disk-shaped specimens
[44]	Epoxy/GF Epoxy/CF	-50 - 125	5 Modulation: ±0.5 [K]	20	TMDSC ASTM E1952-98	Cross-ply samples Disk-shaped specimens Strong temp. dependency of Cp
[43]	Epoxy/CF	-40 - 125	Not mentioned	Not mentioned	DSC	UD samples
[47]	PEEK/CF	20 - 380	For heating: 3 For cooling: 10 Modulation varied between: ±1 and ±0.5 [K]	10 - 12	TMDSC	As-received tapes No information about sample preparation
[46]	PEEK/CF	25 - 300	Not mentioned	Not mentioned	DSC	2 [mm] thick UD samples
[48]	PES/CF	10 - 420	3 ±1 modulation	Not mentioned	TMDSC	3 layered samples processed by TP-AFP
[3]	PP/GF	25 - 250	10	Not mentioned	DSC	DSC of cured and uncured PP, then ROM for composite Cp

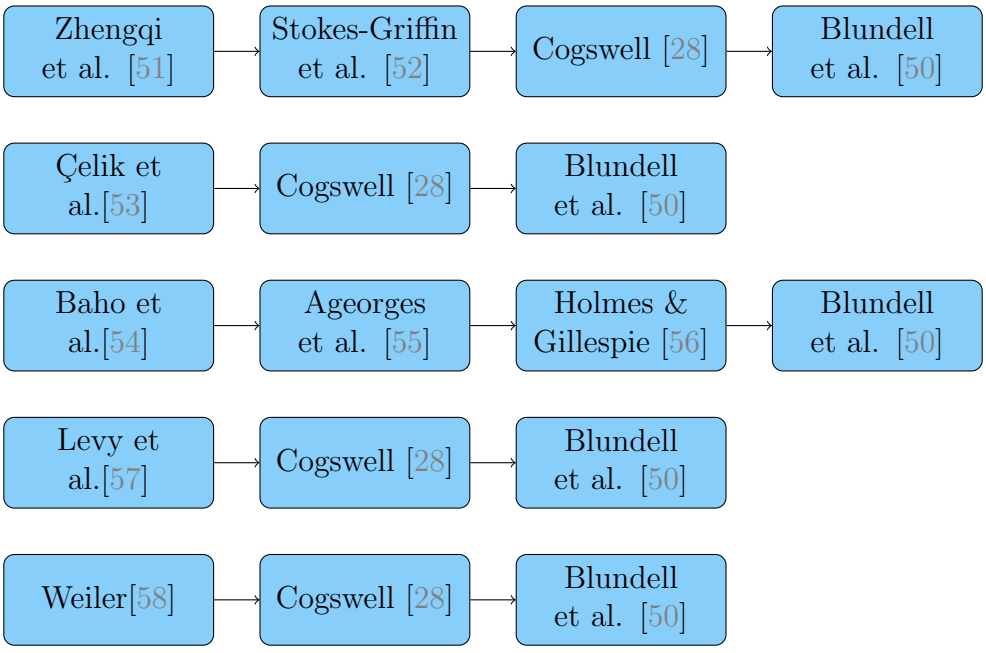

Figure 6: Sequence of specific heat capacity acquisitions

3.2 Manufacturer's recommendation for accurate specific heat capacity measurements

Table 3 below summarizes the recommendations from the manufacturer of the used DSC machine. [59][60]

Table 3: Recommendations from the DSC manufacturer [59, 60]

Recommendations	**Reason**
Sample preparation	
Cover with the sample the bottom of the crucible as much as possible.	To achieve good thermal contact.
Do not crush the samples, rather cut cross sections.	Can introduce thermal history.
Sample size:	
For composites: $>$ 10 mg	
Crucibles:	
Standard pans.	It is important to make sure that the bottom of the pan is not deformed after loading the samples and throughout the measurement to maintain good heat transfer.
Use the same type of pan for all the measurements. (baseline, reference, sample)	To ensure same conditions.
Heating rate:	
Between 10 and 20 K/min.	Dependent on the tested material.
Cell purging:	
Most commonly with Nitrogen with a recommended 50 mL/min.	To create an inert environment in the cell to prevent oxidation and to remove moisture.
Cleanliness:	
It is important to keep the DSC cell free from contamination.	To ensure good quality data acquisition.
Decomposition:	
Avoid decomposition in the DSC cell.	It can contaminate the cell.

4 Materials and methods

The first part of this section entails the tested materials. This includes the description of composite samples, as well as the neat PEEK and pure carbon fiber specimens. The latter two sample types were tested, since many authors have obtained the specific heat capacity of their respective composites using the rule of mixtures as was shown in subsection 1.4. However, no evaluation was found in the corresponding literature, whether this approach provides an accurate prediction. To address this problem, the constituents of the tested composite samples were also subjected to DSC measurements. This tested material section is followed by the corresponding specimen preparations. Lastly, the DSC measurement procedure is discussed.

4.1 Materials tested

4.1.1 Carbon-Fiber Reinforced Poly-Ether-Ether-Ketone

The composite samples tested in this study were fabricated from preimpregnated UD carbon fiber reinforced PEEK (Poly-Ether-Ether-Ketone) tapes (Toray Cetex TC1200 [61]), supplied by Toray industries. It is a high end thermoplastic tape and was chosen due its relevance in the aviation industry. The preimpregnated tapes contain carbon fibers manufactured by Hexcel, of type AS4D with 12K rovings. It is a Poly-Acrylo-Nitrile (PAN) based high strength, high strain continuous carbon fiber.[62] [63] The material is supplied in tapes with a width of 12 inch (304.8 mm), from which individual plies were cut for specimen preparation. The batch id. and the most important material attributes can be found in Table 4.

Table 4: Preimpregnated PEEK/CF tape material data [62] [63]

Tape name	**Manuf.**	**Matrix**	**Fiber**	**Resin content**	**Thickness**	**Batch id.**	**Mfg. date**
Toray Cetex® TC1200	Toray	PEEK	AS4D	34 [%] wt	0.14 [mm]	120619-1TP4-4	10/22/2020

4.1.2 Poly-Ether-Ether-Ketone Granulate

For the specific heat capacity measurements of the neat polymer resin, PEEK 150G [64] samples were obtained from Victrex, which is the same polymer as the matrix material of the tested composites. It is a semi-crystalline aromatic polymer, where the 150 refers to its medium viscosity and G refers to the granulate form. According to the manufacturer, the granulate glass transition temperature (Tg) is 143 °C and its melting point (Tm) is at 343 °C. Table 5 contains the relevant information about the tested polymer.

Table 5: PEEK granulate material data [64]

Polymer name	**Manuf.**	**Tg [°C]**	**Tm [°C]**	**Material form**
PEEK 150G	Victrex	143	343	Granulate

4.1.3 Dry Carbon fiber

In order to obtain the pure carbon fibers, composite tapes were subjected to a polymer burn-off process. The polymer burn-off experiment was carried out using a Carbolite ELF 11/14B Chamber furnace. The relevant furnace characteristics can be found in Table 7. The material used for the experiment was a Suprem AS4/PA12-2159 unidirectional tape, more information about the tape is depicted in Table 6. Attention was given, that the tape contained the same type of carbon fiber(AS4) as the tested composites in this study. The PA matrix material was chosen due to its lower melting point and decomposition compared to PEEK. It allowed the matrix to be fully burned-off without significantly oxidizing the fibers in the non-inert atmosphere. From the tape a small rectangular part was cut out to fit the crucible that was placed in the oven. The heating and cooling rate was the default heating rate of the oven. The maximum temperature was determined based on the work of Gizyński et al.[65]. They analyzed the thermal properties of PA/CF composites by the means of TGA and reported the start of the PA decomposition between 380-400 °C and the maximum mass loss rate was observed at 465 °C. The latter was chosen for this experiment in order to ensure that no polymer residue is present at the end of the burn-off, along with the 5.5 h retention at that elevated temperature.

Table 6: Preimpregnated PA12/CF tape material data [66]

Tape name	**Manuf.**	**Matrix**	**Fiber**	**Resin content**	**Batch id.**	**Mfg. date**
AS4/PA12-2159 0.15 x 150	Suprem	PA12	AS4	45 [%] wt	20122411	2012/06/05

Table 7: Chamber furnace characteristics [67]

Furnace type	**Manuf.**	**Max temp. [°C]**	**Max. power [W]**	**Volume [L]**	**Serial No.**
ELF 11/14B	Carbolite	1100	2600	14	20-903475

4.2 Sample preparation

The reviewed literature (section 3) provided no standardized specimen design nor investigated its impact regarding the composites. As a result, various sample types have been produced from the CF/PEEK composite material in order to investigate the influence of different sample preparation on the resultant specific heat capacity as shown in Figure 7. Five different specimen designs were tested for the CF/PEEK composite material system: as received tapes, 3ply and 4ply consolidated samples with unidirectional layup, 7ply samples with asymmetric cross ply layup and powder samples. The samples with increasing ply counts were tested with the aim of identifying the impact of mass and sample thickness on the measurement results.

The as-received tapes as well as the 4ply and 7ply samples were prepared in two ways: one set in an approximate rectangular shape, while the other set was prepared in the standard disk shape used for all the other specimens. This was done to asses the significance of maximizing the thermal contact area between the pan and the samples on the specific heat capacity results. Last but not least, powder samples were also prepared. The motivation behind this was to prepare a sample type that better represents the average composite material, since previous studies have noted the difficulty of obtaining representative samples. This is attributed to the small size of the specimens, which can contain variations of fiber-rich or polymer-rich regions that do not reflect the overall composite. To achieve this, powder was collected from milling the surface of a composite laminate made from the same tape material as the other samples. Prior to the powder collection, the milling area underwent thorough cleaning to ensure the exclusion of any foreign material.

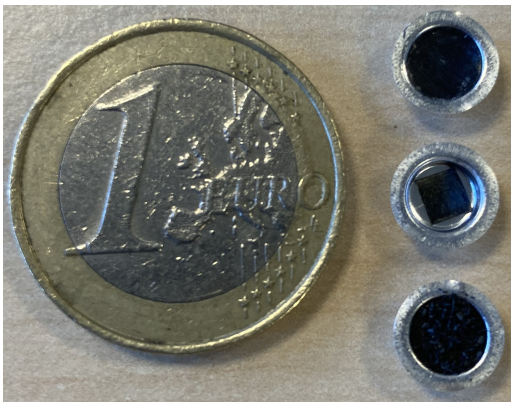

Figure 7: Tested sample preparations, disk shaped(top), approximate rectangular shape (middle), powder(bottom)

In order to obtain the layered samples, three laminates were manufactured using a picture frame mould with dimension of 300 x 300 mm^2 in all cases. All laminates were consolidated using a press-cycle according to the procedure shown in Table 8. Circular disks with a diameter of 4.9 mm were CNC precision milled from the laminates and carefully deburred using sandpaper. Finally, the solid samples were thoroughly washed with isopropanol to remove any contamination from the surfaces before the measurement.

Table 8: Consolidation parameters

Material	Toray Cetex® TC1200
Pressure pre heat [bar]	2
Pressure main [bar]	20
Dwell preheat time [min]	30
Dwell main time [min]	30
Temperature [°C]	380
Heating rate [°C/min]	10
Cooling rate [°C/min]	5

The pure polymer granulate required no pre-processing prior to characterization and was tested as-received. The obtained carbon fibers from the polymer burn-off were cut approximately to size of the measuring pans, then were compacted into the crucibles with the help of a rod.

A summary of the tested samples types and their relevant information regrading the DSC measurements are shown in Table 9. In the remainder of this study, tape denotes the as-received tapes in an approximate rectangular shape, while 1ply refers to the as-received tapes in a disk shape. 4ply and 7ply denote the disk-shaped samples, while 4ply unordered and 7ply unordered refer to the approximate rectangular shape.

Table 9: Tested sample types

Sample type	**Material**	**Sample shape**	**Layup orientation**	**No. samples**	**Avg. weight of the samples [mg]**
Tape	Toray TC1200	Rectangular	[0]	3	2.39
1ply	Toray TC1200	Disk	[0]	6	4.53
3ply	Toray TC1200	Disk	$[0]_3$	3	13.18
4ply	Toray TC1200	Disk Rectangular	$[0]_4$	12 3	17.41 10.13
7ply	Toray TC1200	Disk Rectangular	[0/90/0/90/0/90/0]	12 3	29.99 18.34
Powder	Toray TC1200	Solid/Disk	[0]	3	19.78
PEEK granulate	Victrex 150G	Solid/Granulate	-	9	16.30
Carbon fiber	AS4	Solid/Fiber	-	9	-

4.3 DSC measurement procedure

The measurements included in this study were carried out with a TA instruments Discovery 250 DSC machine available at the University of Twente laboratory. The ASTM E1269-11 standard was followed for the determination of the specific heat capacity.[34], detailed in subsection 2.1. The reference material was synthetic sapphire(Al_2O_3) weighing 26 mg, provided by the manufacturer of the DSC machine. The measurements were carried out under a constant 50 mL/min nitrogen purge. Standard Tzero aluminum pans (P/N 901683.901) were used in all of the experiments, along with either Tzero lids (P/N: 901671.901) or Tzero hermetic lids (P/N: 901684.901), depending on their availability in the laboratory. Whenever either the Tzero lid or Tzero hermetic lid was available, all measurements (baseline, reference, and sample runs) were carried out using the same type of lids.

The applied temperature program consist of 8 segments, depicted in Figure 8. Starting with a 10 [min] equilibrium at 40 °C, then heating up the 380 °C. This temperature was chosen to fully melt the PEEK polymer, but to avoid thermal degradation. The aim was to obtain specific heat capacity values over a wide temperature range, providing data for process simulations. This was followed by a 10 min isothermal step to ensure, that equilibrium has been reached and all the samples start the next segment from the same temperature. The next step was cooling back down to 40 °C. This thermal cycle was repeated once again. Employing two identical thermal cycles subsequently was chosen, since the first one served to erase any prior thermal history of the samples, and to ensure proper thermal contact between the sample and the crucible, while the second cycle was used for heat capacity determinations.

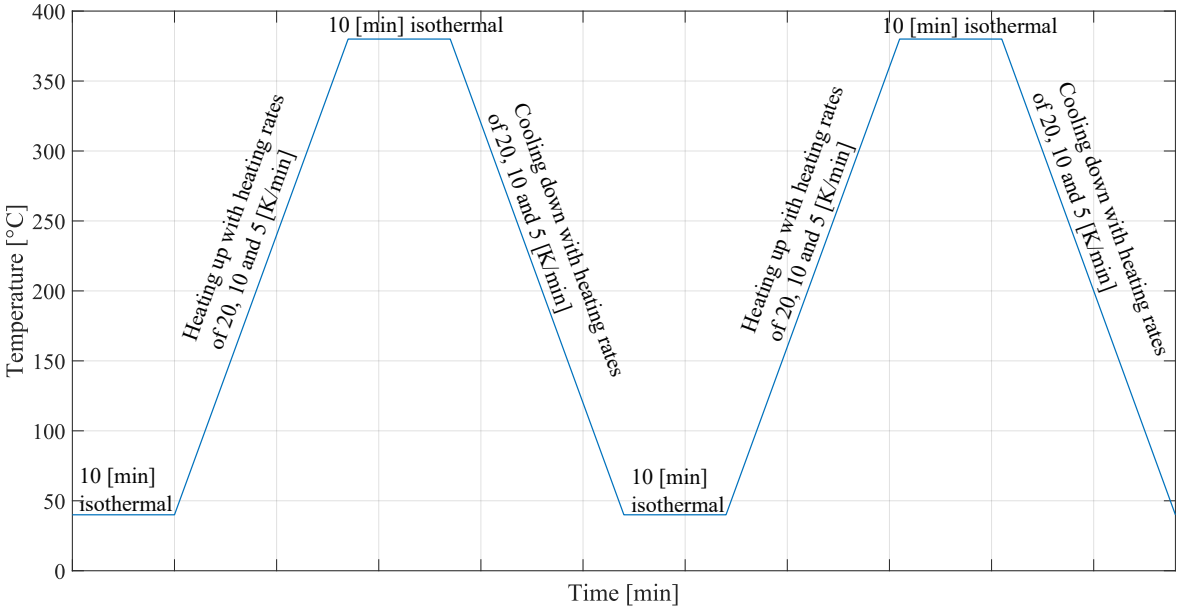

Figure 8: Temperature program of the DSC experiments

During the first set of measurements, the heating rate was set to 20 K/min, following the ASTM standard. Additionally, heating rates of 10 and 5 K/min were also tested to investigate the effect of thermal lag within the samples. The 4-ply and 7-ply samples were chosen for this purpose, as they are the thickest and heaviest samples, resulting in the most pronounced thermal gradient.

For the first set of experiments, the baseline and sapphire runs were completed before all the samples were measured and once again after the entire batch of samples was done. By measuring the baselines before and after, a possible temporal shift in baseline consistency could be captured. They were repeated five times in both cases to assess repeatability of the equipment.

However, for all the consecutive measurements with heating rates of 20, 10 K/min and 5 K/min, the baseline and sapphire runs were conducted both before and after each different type of sample was tested. Table 10 provides the details of the tested samples and their corresponding measurement parameters.

Table 10: Sample types and heating rates

Sample type	**Sample shape**	**Heating rate [K/min]**	**No. samples**
Tape	Rectangular	20	3
1ply	Disk	20	3
3ply	Disk	20	3
4ply	Disk	20	6
4ply unordered	Rectangular	20	3
7ply	Disk	20	6
7ply unordered	Rectangular	20	3
Powder	Solid/Disk	20	3
Carbon fiber	Solid/Fiber	20	3
4ply	Disk	10	3
7ply	Disk	10	3
PEEK granulate	Solid/Granulate	10	3
Carbon fiber	Solid/Fiber	10	3
4ply	Disk	5	3
7ply	Disk	5	3
PEEK granulate	Solid/Granulate	5	3
Carbon fiber	Solid/Fiber	5	3

5 Results

In subsection 5.1 the consistency of the baseline heat flow over time is presented and its influence on the heat capacity results. It is followed by the impact of sample preparation on the measurements in subsection 5.2. In subsection 5.3 the effect of the temperature program and thermal history is discussed, followed by the influence of the heating rate on a selected number of sample types in subsection 5.4. Moreover, the application of the rules of mixtures on the heat capacity is presented in subsection 5.5. Lastly, the results are compared to literature and some uncertainties during the DSC runs are highlighted in subsection 5.6 and in subsection 5.7 respectively.

Figure 9 shows an exemplary result of the heat capacity measurement using the three run method according to the ASTM E1269 standard [34]. The measurements of the baseline, reference and sample heat flows were carried out sequentially. As mentioned in subsection 2.1, two heat flow differences are needed to obtain the specific heat capacity of the composite samples: one between the baseline and sapphire heat flow curves labeled as Dst, and the other between the baseline and sample heat flow curves labeled as Ds.

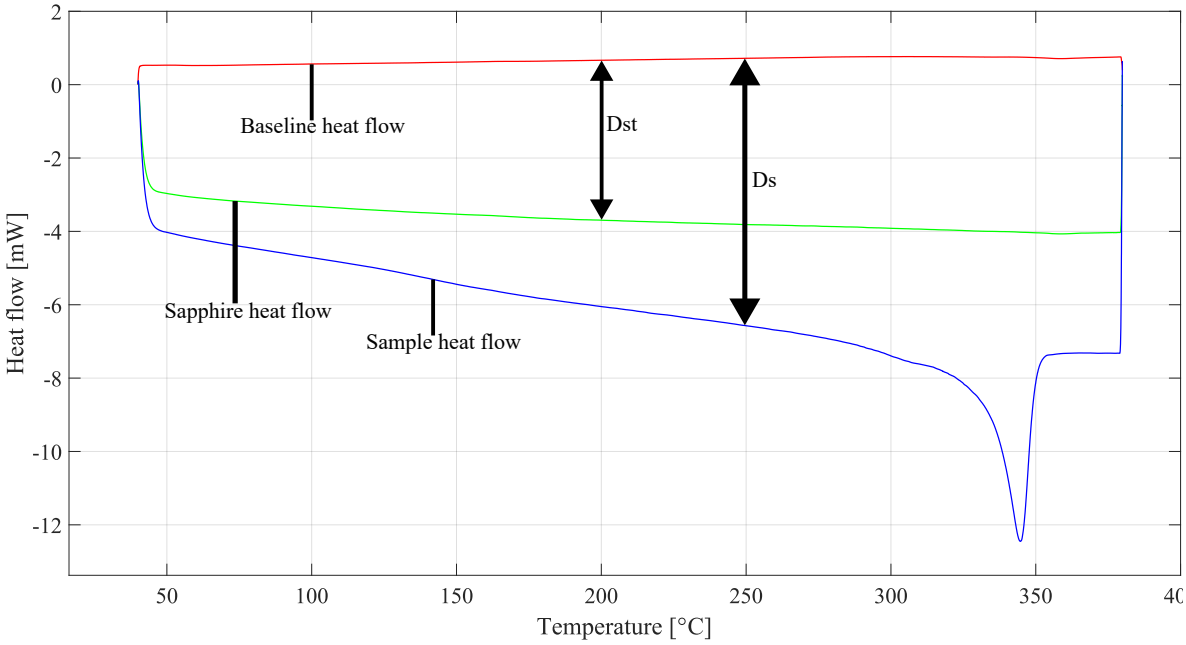

Figure 9: Typical result of the heat capacity measurement using DSC upon heating

5.1 Baseline consistency

Figure 10 shows the average heat flows of the five baseline and sapphire measurements carried out prior to the sample measurements and after all the sample measurements had been completed. A consistent shift of roughly 1 mW can be observed in both cases. The results of the five subsequent baseline measurements are in close agreement with each other within 0.05 mW and 0.1 mW, for the baseline runs done prior and after the

sample measurement respectively, exhibiting high reproducibility. The observed drift in the baseline and sapphire measurements is likely a consequence of other DSC measurements inserted into the sequence by different researchers or can also be attributed to the gradual contamination originating from the samples employed in this study. Nevertheless, this showcased baseline shift had a significant effect on the resultant specific heat capacities, which will be explained in the remaining part of this section.

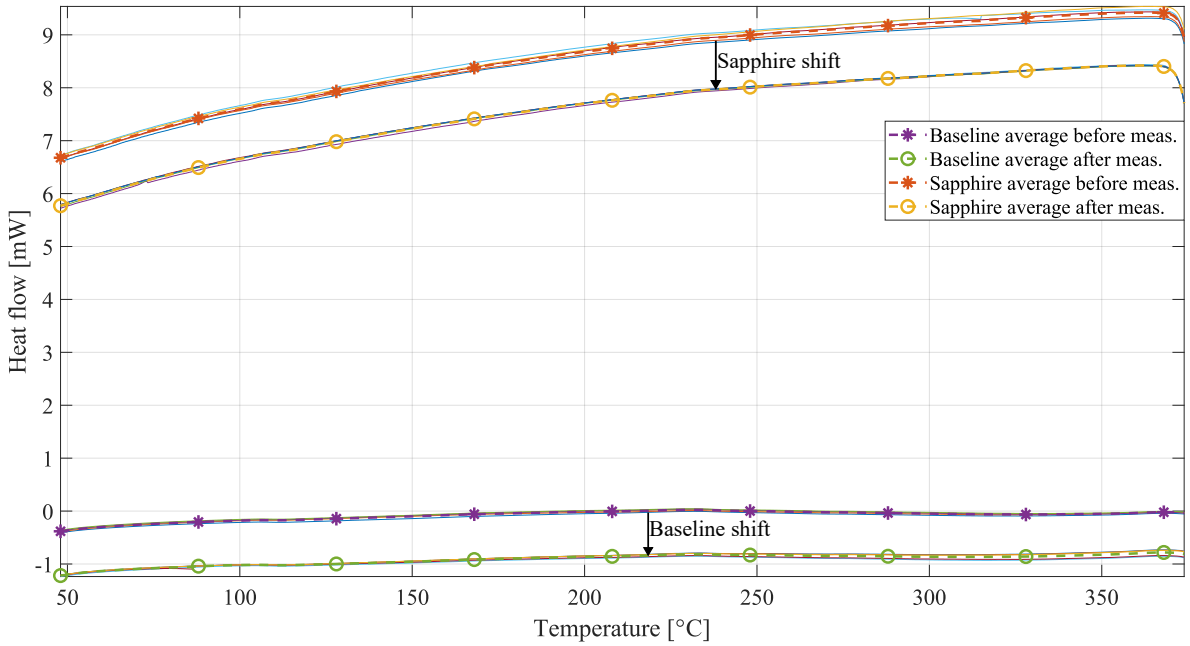

Figure 10: Baseline and sapphire heat flows before and after the sample measurements

As detailed in subsection 2.1, two heat flow differences are required for the heat capacity determination. The first one is between the baseline and sapphire heat flows. Given that both mentioned heat flows have shifted with approximately the same magnitude, their differences have not changed significantly, less than 2.5 % over the entire temperature range, which is within the machines guaranteed precision. However, regarding the second heat flow difference, between the baseline and the sample heat flows, this drift had a significant effect. The heat flow curves for the tested samples increase with increasing sample weight. As such, the lighter samples are more affected by the same 1 mW baseline drift than the heavier samples.

For instance, the lightest 1ply sample had heat flow values between 0.8 mW and 2.4 mW at their lowest and highest temperatures respectively. Therefore, their results are comparable to the magnitude of the baseline shift, making a substantial impact on their resultant heat capacities. This can clearly be seen from Figure 11, showing the the calculated specific heat capacities per sample type by using the baseline average before and after the sample measurements and taking their percentage change. In the case of 1 ply samples this percentage change of the specific heat capacity reaches almost 70 % at 80 °C, which decreases to 35 % at 365 °C.

As the weight increases, with higher layer count, this drift becomes less pronounced. However, even with the heaviest 7ply samples with heat flows between 9 and 17 mW at their lowest and highest temperatures respectively, this baseline drift still makes a notable influence between 9 % and 7 % at 80 °C and 365 °C respectively.

It should be noted that the tape results, the lightest sample types with the lowest heat flow values were omitted from this bar plot for better readability. This was done, since the baseline heat flows completed prior to the sample measurements cross the heat flow curves of the tape measurements at around 160 °C rendering their difference to zero. Therefore, the resultant specific heat capacities also become almost zero resulting in percentage changes in the range of 500 - 1000 %.

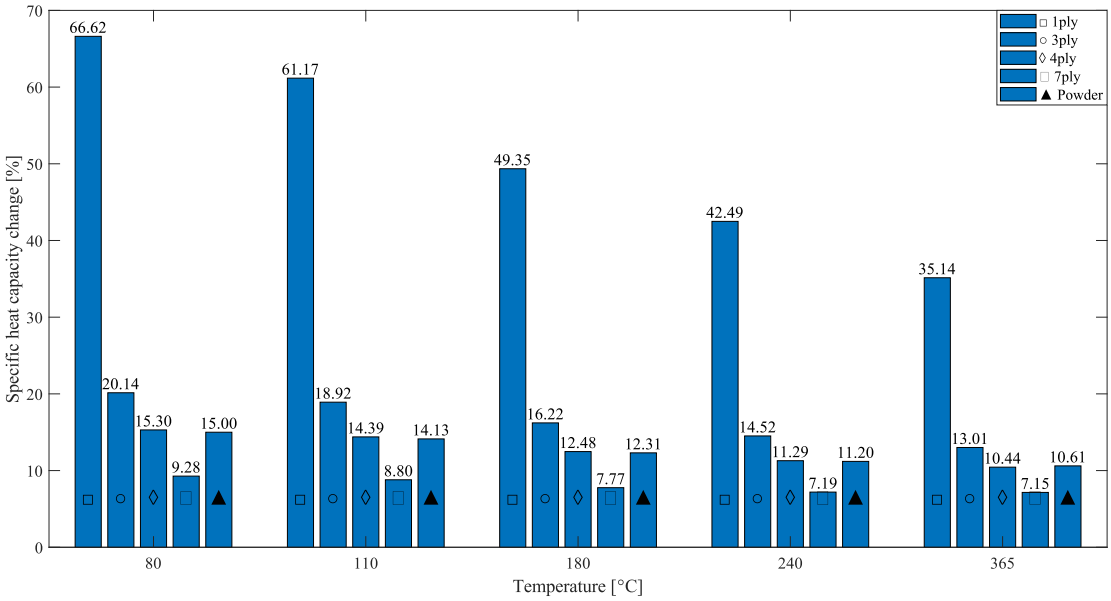

Figure 11: Influence of baseline shift on the resultant specific heat capacities

In order to mitigate the influence of the above mentioned baseline drift, the subsequent DSC experiments were carried out with baseline measurements before and after testing each different sample type to closely monitor their consistency. Figure 12 displays the percentage change of the resultant specific heat capacities per sample type. The basis of the percentage change is the two specific heat capacities obtained by using the baseline done prior to each different sample runs and by using the baseline completed after each different sample measurements, for every sample type. It was noted, that the baseline drifted significantly less throughout the second measurement sequence, hinting towards that the pronounced baseline drift in the first set of measurement were likely the consequence of foreign DSC runs inserted into the running sequence. Moreover, the frequent baseline measurements effectively constrained this shift into smaller portions across the different sample types. Therefore, the shift's impact on the sample results was not as significant as in the first experiments. In the case of the 4ply samples, the percentage change of the specific heat capacity results were reduced from 15 % to less than 1 % at 80 °C and from 10 % to 0.7 % at 365 °C. The same trend can be observed in the 7ply results as well, however the reduction is less pronounced in this case.

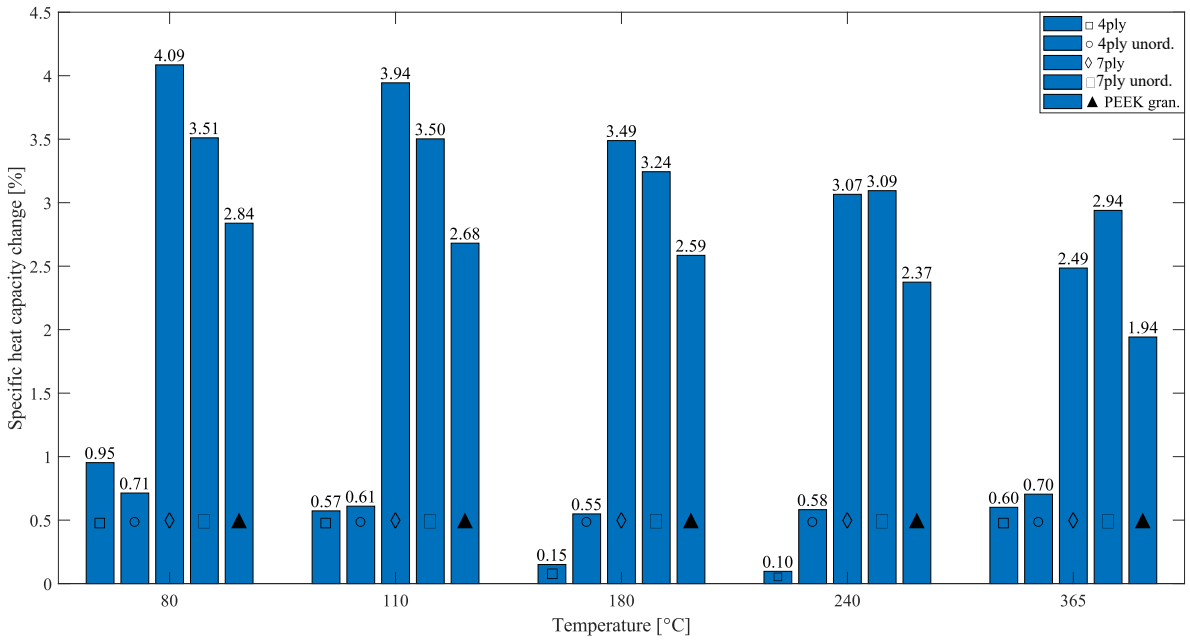

Figure 12: Influence of frequent baseline measurement on the resultant specific heat capacities

To conclude, the shift in baseline measurements can significantly influence the resultant specific heat capacities. Therefore, it is crucial to perform baseline measurements frequently in order to check their consistency, and if any notable shift is observed, action can be taken. Furthermore, based on the results of the first set of measurements, it is advisable to opt for heavier sample weights. These samples yield larger heat flow values, rendering them less susceptible to baseline deviations. However, continuously increasing the sample wight poses new challenges in heat capacity measurements, such as the accumulation of thermal gradients within the samples, which will be addressed later in this study.

5.2 Influence of sample type

This section discusses the influence of the sample mass and form as well as the impact of sample shape on the resultant specific heat capacities.

5.2.1 Influence of sample mass

Figure 13 shows the specific heat capacities of the tested samples as a function of weight at various temperatures, employing a heating rate of 20 K/min, the dotted lines connect the data points corresponding to the same temperature. Each curve corresponds to a specific temperature, ranging from 60 °C to 365 °C, covering the entire measurement range. The results represent the averages of three separate sample measurements, with error bars depicting the standard deviations. Figure 13 clearly illustrates that both the tape and 1ply samples, with the lowest masses, consistently yield lower heat capacities across the entire temperature range compared to the layered

samples. In the case of 3ply, 4ply, and 7ply specimens, their resultant heat capacities exhibit close agreement throughout the measured temperature range, with only a slight increase observed at higher temperatures with increasing ply count. It is interesting to note that the heat capacity steeply increases between the tape, 1ply and 3ply samples. However, as the sample weight approaches that of the 3ply samples, this steep increase flattens out with further added weight. These observations suggest that the sample mass had a substantial effect on the results. Furthermore, as mentioned in subsection 4.2, the 3ply and 4ply samples have a unidirectional layup, while the 7ply samples have an asymmetric cross-ply layup configuration. From Figure 13, it can be concluded, that the layup orientation had no significant impact on the resultant heat capacities, comparable values were obtained in both cases.

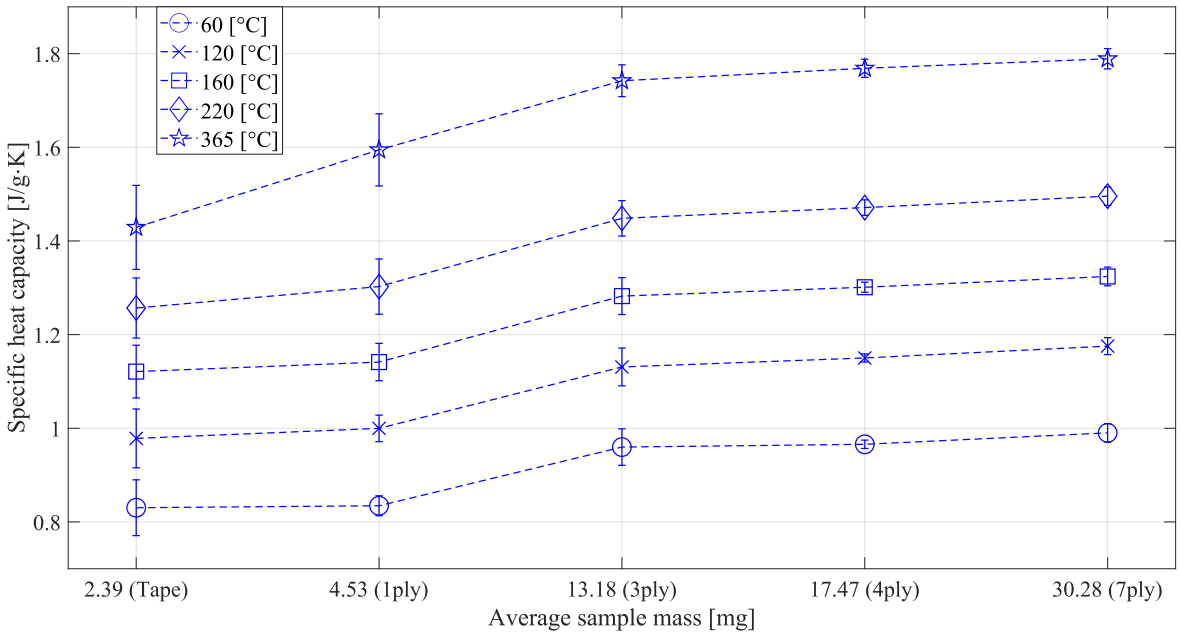

Figure 13: Influence of sample mass

5.2.2 Influence of sample shape

Figure 14 illustrates the influence of sample shape and form on the resultant specific heat capacities with a 20 K/min heating rate. The graph indicates that variations in sample shape (disk vs unordered) for 4ply samples resulted in slightly lower heat capacities at higher temperatures, however it is a marginal difference indicated by the overlap of the corresponding error bars. Similarly, in the case of 7ply samples, the change in specimen shape had very little effect on the results. Regarding the sample form, the powder samples performed well, with their heat capacity results closely comparable to the layered results. The only discrepancy is encountered after the full melting of the specimens. However, even in this case, there is a slight overlap of the error bars, indicating a non-significant difference.

Moreover, the graph suggests that the mass of the specimens had a more substantial impact on the resultant heat capacities than the sample shape or form. Upon examining the specimen weights, it becomes apparent that once their mass reaches the weight of the 4ply disk-shaped samples, the results showcase a good agreement regardless of the shape or even the form (layered vs powder) of the specimen.

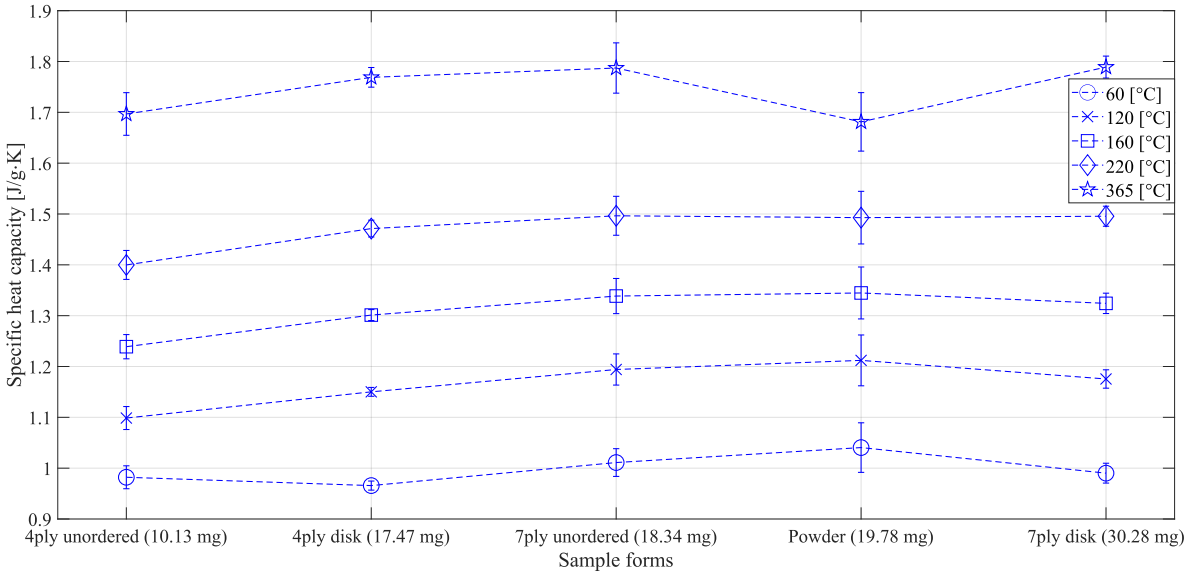

Figure 14: Influence of sample shape

5.2.3 Spread of the results

Figure 15 shows the calculated coefficient of variation for the tested sample types. For each sample type three specimens were measured. This analysis aimed to assess the consistency of the results across different sample types. Figure 15 reveals that tape samples yielded the most inconsistent data across the entire temperature range, followed by the 1ply samples. The 7ply unordered samples showed closely comparable heat capacity values to their disk-shaped counterparts. However, their results exhibited notably higher scatter. A similar trend can be observed in the case of powder samples, which, despite exhibiting heat capacity values in close agreement with the layered specimens, showcased notably higher variability. Interestingly, this higher variability closely resembles that observed in the unordered 7ply samples. In contrast, the 4ply unordered samples exhibited significantly lower variability. However, their obtained heat capacity results were slightly lower than those of the disk-shaped specimens, as was shown above.

Among the three disk-shaped samples with increasing ply count, the 3ply specimens displayed higher scatter in their results compared to the 4ply and 7ply samples. This suggests that a further increase in sample weight reduces measurement variability, with the most consistent data obtained from the heaviest disk-shaped samples, namely the 4ply and 7ply specimens.

Consequently, these findings indicate that shape of the samples, as well as different forms, such as powder, are capable of yielding similar results that of the disk-shaped specimens. However, the key difference lies in the consistency of the obtained results, which is notably lower, when disk-shaped samples are employed. This implies that more precise and consistent measurement results can be obtained with this specimen shape. Therefore, the 4ply and 7ply samples were chosen as the preferred sample types for further investigating the influence of the applied heating rate, enabling a reduction in the number of sample types, which would have otherwise resulted in an impractical number of measurements for this study.

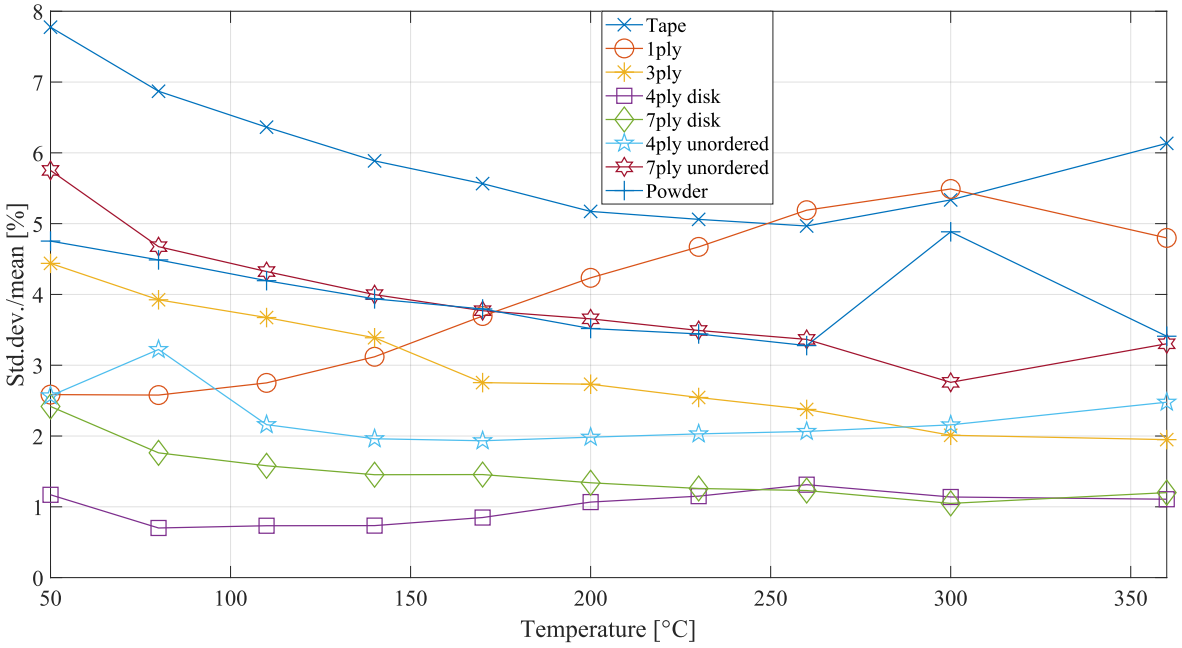

Figure 15: Coefficient of variation per sample type

5.3 Influence of the thermal cycles

As mentioned in subsection 4.3 all DSC experiments were carried out with the same temperature program consisting of two identical thermal cycles. In the following section, the influence of the applied temperature program will be explored using the 1ply and 7ply samples. They were chosen because the 1ply samples were tested in the same state as received from the manufacturer, while the 7ply samples had undergone press consolidation to form layered specimens before being measured with DSC. This approach allows the influence of the temperature program to be assessed on sample types with different thermal histories. Moreover, in subsubsection 5.3.1 the crystalline content of the samples from the first and second cycle was calculated in order to assess whether any significant change has occurred which in turn could change the resultant specific heat capacities.

Figure 16 shows the specific heat capacity curves of the 1ply samples obtained from the first and second heat up cycles with 20 K/min heating rate. The specific heat capacity curves are the averages of 3 separate sample measurements, the bands depict the standard deviations. As can be seen from Figure 16 the 1ply samples in the first heat up cycle go through a sharp glass transition between around 139 °C and 146 °C, which is followed by a pronounced cold crystallization between 160 °C and 190 °C. These kinetic phenomena cannot be observed in the second cycle. It can also be seen from Figure 16, that the melting peak shifted to a lower temperature in the second cycle from around 343 °C to around 341 °C. Moreover, the melting peak in the second cycle has a significantly higher value of 2.56 J/gK compared to 1.94J/gK in the first cycle. Consequently, the absence of glass transition and cold crystallization in the second heat up cycle hints towards the increased crystalline content present in the PEEK matrix in the second thermal cycle. Lastly, it is apparent from Figure 16, that the specific heat capacity from the second cycle is notably higher over the entire temperature range compared to the first cycle.

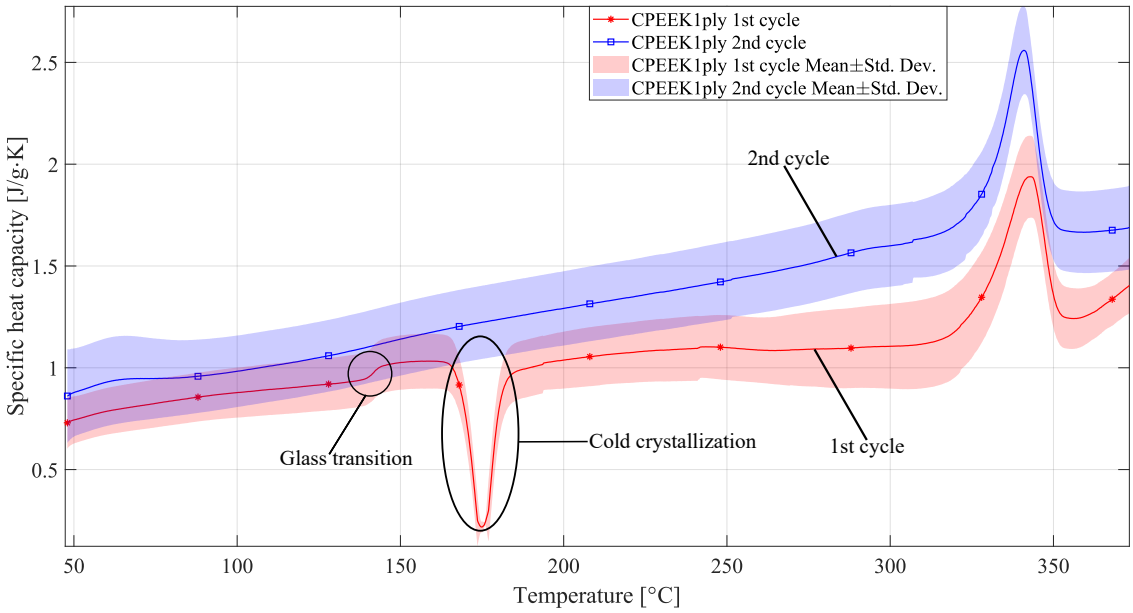

Figure 16: Specific heat capacity results of the the as received tapes obtained from the first and second heat-up cycle

Figure 17 displays the specific heat capacity of the 7ply samples obtained from the first and second thermal cycle upon heating. As can be seen from Figure 17, the specific heat capacities from the first and second thermal cycles coincide very well from 40 °C until the glass transition. Above the glass transition region, the heat capacity from the second cycle starts to slightly surpass the heat capacity from the first cycle, which trend abruptly reverses and the heat capacity curves cross each other at 301 °C. It is interesting to note, that the kinetic events, which occurred in the case of as received tapes such as the sharp glass transition and cold crystallization did not occur in the layered samples. Last but not least, the layered samples exhibit a double melting peak during the first heating cycle, a feature that is absent during the second heating cycle.

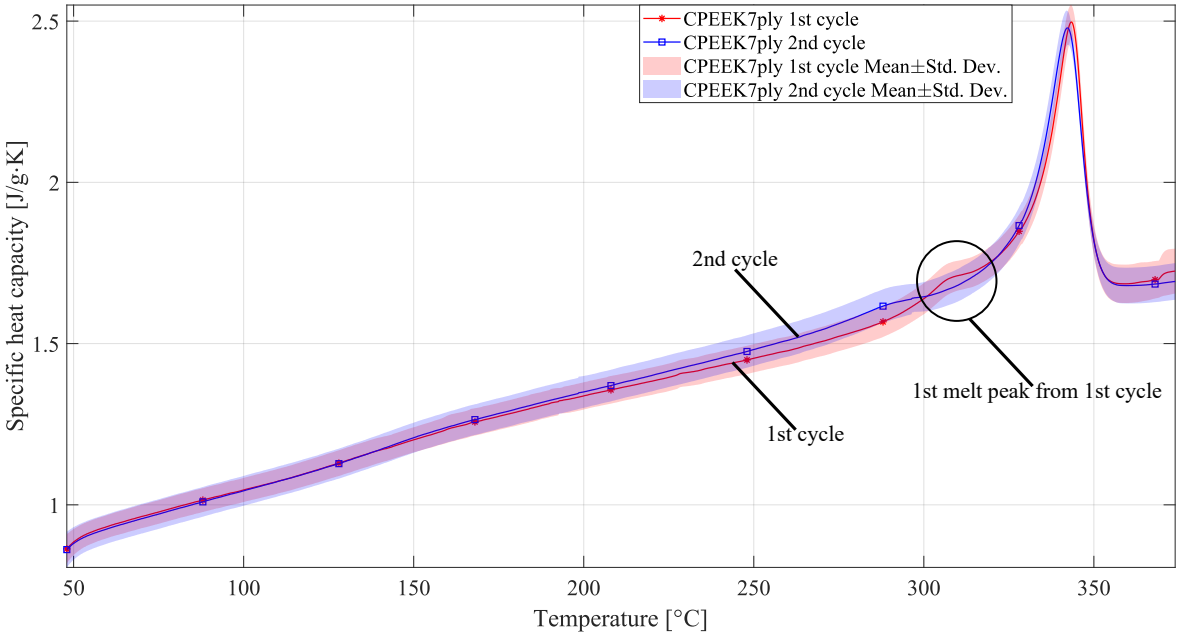

Figure 17: Specific heat capacity results of the the 7ply samples obtained from the first and second heat-up cycle

It can also be seen from Figure 17 that the sharp, more pronounced melting peak from the first cycle is at a slightly higher temperature at around 343.4 °C with slightly higher value of 2.5 J/gK compared to the melting peak form the second cycle which is at around 342.3 °C with 2.48 J/gK. In addition, it is worth noting that the standard deviations bands of the 7ply and 4ply (shown in subsection A.3) samples are significantly narrower that of the 1ply samples indicating more repeatable results.

5.3.1 Crystalline content

The change in the polymer microsturcture due to the thermal cycles can significantly alter the heat capacity results as was detailed in the work of Khalaf et al.[68]. The authors observed a notable decrease in heat capacity values of polyethylene samples with increasing crystallinity. As a result, the degree of crystallinity (DOC) has been calculated from the melting peaks of the first and second heating cycle in order to investigate if any notable change has taken place in the crystallinity content of the samples which could could potentially account for the deviation in specific heat capacity values obtained from the first and second heat up cycle. For the crystallinity calculation one needs to construct a baseline first which would be the heat flow curve of the samples if no transition were to take place. The peak integration to obtain the melting enthalpy is then carried out within the baseline limits. Regarding the consolidated samples, linear baselines were employed. However, in the case of the as received samples, the baselines were chosen to be tangential sigmoidal baselines according to the recommendations by the DSC manufacturer.[69] It was stated, if the heat flow curve is not flat but has a slope to it before and after the transition, a tangential sigmoidal baseline should be

used for accurate calculations. The limit temperatures for the peak integration have been chosen to be 275 °C and 360 °C and were kept the same for all samples in order to incorporate the double melting peaks exhibited by the consolidated samples in the first heat up cycle. With the obtained melting enthalpies one can calculate the degree of crystallinity of the sample by using the equation below:

$$Xc(\%) = \frac{DHm - DHcc}{(1 - w) * DHOf} * 100, \tag{6}$$

where DHm is the enthalpy of melting, DHcc is the enthalpy of cold crystallization, DH0f is the enthalpy of fusion of a completely crystalline polymer and finally w is the weight fraction of carbon fiber in the sample. It is worth noting that in the case of 1ply samples the enthalpy from the cold crystallization in the first heat up cycle has to subtracted from the melt enthalpy to obtain the true degree of crystallinity. The enthalpy of fusion of the complete crystalline PEEK has been obtained from the open literature with a value of 130 J/g [70]. Table 11 shows the calculated crystallinity results.

Table 11: Degree of crystallinity from the first and second heat-up

	Heating rate [K/min]	**DOC 1st cycle avg. [%]**	**Std. dev.**	**DOC 2nd cycle avg. [%]**	**Std. dev.**
1ply	20	12	3.3	25	0.89
4ply	20	39	0.65	38	1.1
7ply	20	35	0.91	34	0.43

As it was expected the average crystalline fraction of the as received samples in the first thermal cycle was 13 %, which increased up to 25 % in the second heat up cycle. Regarding the consolidated 4ply and 7ply samples, the average crystallinity did not change notably throughout the temperature cycles only a slight decrease can be observed. It is interesting to note that the 4ply samples showcase a slightly higher crystalline content in both thermal cycles 38 % and 39 % for the first and second cycle respectively compared to the 7ply samples 35 % and 34 % average crystallinity from the first and second cycle respectively.

5.4 Influence of heating rate

Figure 18 shows the specific heat capacity curves of the 4ply samples, and 7 ply samples at different heating rates. The maximum tested heating rate was 20 K/min according to the ASTM standard [34] and subsequent measurements have been carried out with decreased heating rates of 10 and 5 K/min in order to explore the influence of heating rate on the resultant specific heat capacities. The specific heat capacity curves are the averages of 3 separate sample measurements, the standard deviation bands have been omitted from the graph for better readability. The results with depicted standard deviations per sample type at different heating rates can be found in subsection A.4.

In the case of 4ply samples as shown in Figure 18a, measurements with heating rates of 5 and 10 K/min result in nearly identical specific heat capacities. Using the ASTM [34] recommended 20 K/min heating rate, the obtained heat capacities deviate significantly, yielding considerably lower values by 20 - 28 % across the entire temperature range. It is interesting to note, that the 4ply samples subjected to a 20 K/min heating rate yield even lower heat capacity values than of the 7ply samples at the same heating rate.

Regarding the 7ply samples as shown in Figure 18b, a different trend can be observed. In this case the heat capacity curves obtained at 20 and 10 K/min heating rate coincide well, resulting in a maximum of 2 % deviation until the melt region. It is interesting to note that the slight difference between the curves gradually decreases as the temperature increases and the curves nearly match perfectly from 310 °C onward, even after complete melting. Conversely, the specific heat capacity results obtained with 5 K/min heating rate, visibly exceeds both heat capacity curves (with higher heating rates) across the entire temperature range with a slight increase in the difference observed at higher temperatures.

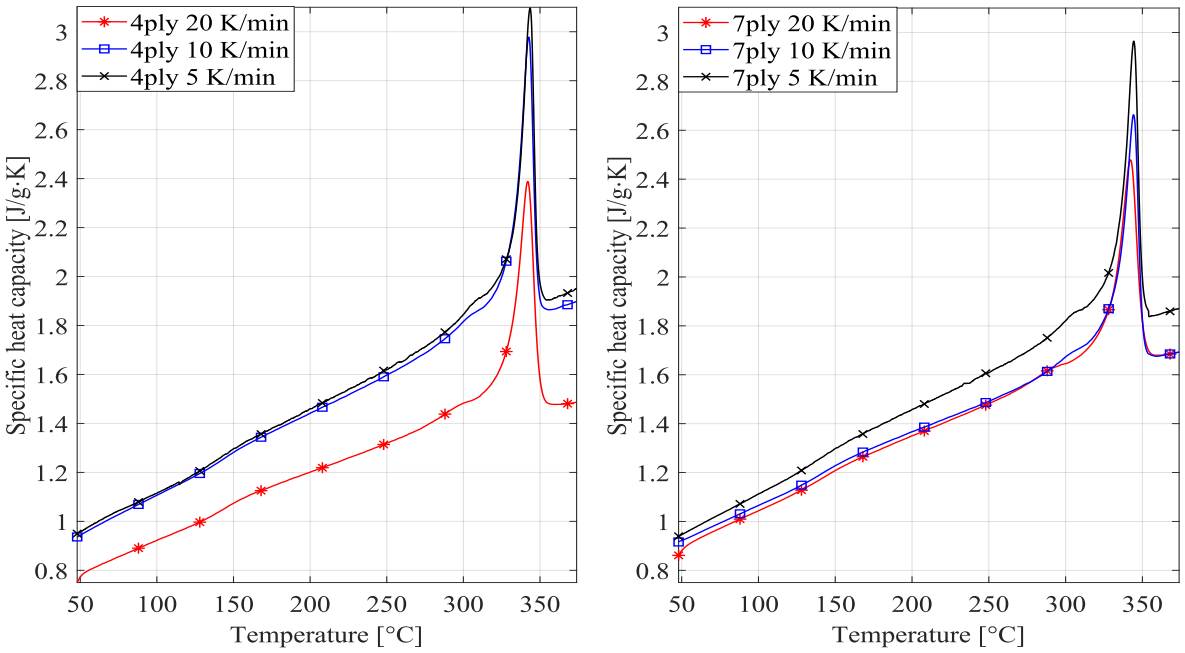

(a) Influence of heating rate on the 4ply samples

(b) Influence of heating rate on the 7ply samples

Figure 18: Influence of heating rate on the specific heat capacities

It is evident from the graphs and the above-mentioned observations, that as the sample weight increases one needs to apply lower heating rates in order to achieve comparable, high heat capacity results. In the case of 4ply samples with and average weight of 17.4 mg employing 10 K/min heating rate already produces heat capacity values in good agreement with those obtained at 5 K/min. In contrast, the 7ply samples with an average weight of 29.3 mg require a minimum heating rate of 5 K/min to

match the results achieved by the 4ply samples at 10 and 5 K/min. This supports the concept that, as the sample weight increases a more pronounced temperature gradient accumulates within the samples. Particularly in the case of poor thermal conductors such as the analyzed composite samples in this study, due to their polymer matrix, necessitating lower heating rates in order to eliminate this unwanted phenomenon and to obtain reliable results.

In order to determine how the temperature gradient in the samples affects the resultant specific heat capacities, one has to look at the heat flows obtained at various temperatures with different heating rates. Figure 19a shows the baseline corrected average heat flows for the 4ply samples normalized by mass, while figure Figure 19b depicts the baseline corrected average heat flows for the 7ply samples normalized by mass.

In an ideal situation the heat flow linearly increases with increasing heating rate, in order to obtain the same specific heat capacities as can be derived from Equation 5. If we can accept the fact that with the lowest heating rate (5K/min) applied in this study is sufficiently low enough that the temperature gradients in the samples can be negligible then one can extrapolate what heat flows should be expected at higher heating rates, which is shown as the dashed lines in Figure 19. The deviation of the experimental curves from these ideal curves can be interpreted as the samples inability to absorb sufficient amount of heat in a limited time frame, which would be needed to uniformly increase the temperature of samples through their whole thickness. It can be seen from Figure 19a that in the case of 4ply samples the experimental curves more or less follow this trend until 10 K/min. Above 10 K/min a visible deviation can be seen between the ideal and experimental curves, which become more pronounced as the heating rate increases indicating a more pronounced temperature gradient accumulation. In the case of 7ply samples as shown in Figure 19b even at 10 K/min heating rate a significant difference can be observed between the ideal and experimental curves which coincides with the fact that with increasing samples mass the temperature gradient occurs already at lower heating rates.

Moreover, by looking at the curves obtained at different temperature it can also be seen that this deviation increases with higher temperatures. Thus, it can be seen that the temperature gradient is not only a function of the heating rate but also a temperature-dependent variable. Last but not least, constructing these curves can serve as a useful tool for selecting the optimal heating rate for heat capacity determination in order to ensure that the influence of temperature gradients within the samples can be minimized.

Consequently, the best matches among the measurements, characterized by the highest values and the lowest standard deviations, are the heat capacities of the 4-ply samples with 10 K/min and 5 K/min heating rates, as well as the heat capacities of the 7-ply samples with a 5 K/min heating rate. Figure 20 shows these results plotted in graph. The largest observed difference is between the heat capacities of the 4-ply samples at 10 K/min and the 7-ply samples at 5 K/min. However, this difference does not exceed 0.02 J/gK, resulting in a mere 1.5 % deviation. These curves are deemed to be the true heat capacity values of the CF/PEEK composite samples and will serve as a basis for comparison with results from other studies available in the existing literature in subsection 5.6.

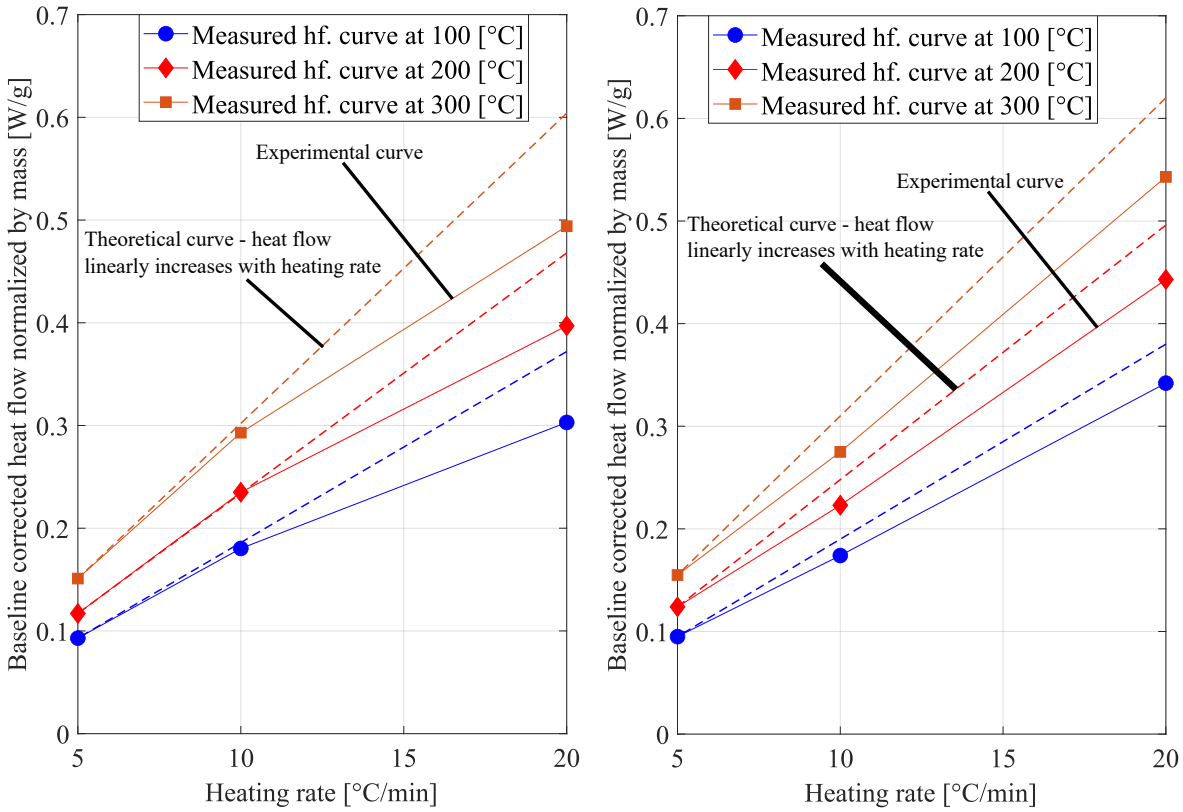

(a) Heat flow deviation 4ply samples (b) Heat flow deviation 7ply samples

Figure 19: Deviation of the baseline corrected average heat flows from the theoretical curves at various temperatures

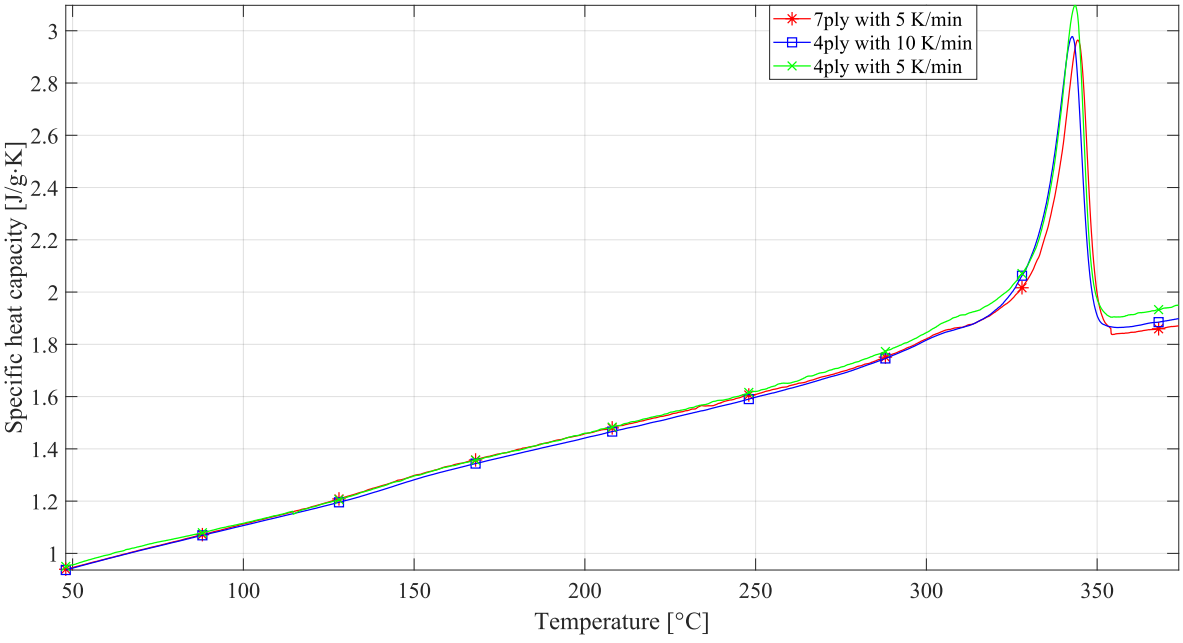

Figure 20: Best matches of the heat capacity results with different heating rates

5.5 Rule of Mixtures

Figure 21 shows the specific heat capacities of the CF/PEEK composite, from its constituent materials using the mixture rule. The plotted curves represent the resultant composites heat capacities calculated from the averages of three independent measurements for both neat PEEK and pure carbon fibers. For better readability the standard deviation bands have been omitted from the graph. The results with standard deviation bands can be found in subsection A.6. The measured specific heat capacities of the neat PEEK and dry carbon fibers are shown in subsection A.5. For the ROM calculation the heat capacity results of the neat PEEK matrix with 5 K/min heating rate were utilized. This was chosen after a comparison of the specific heat capacities of neat PEEK samples at various heating rates to the heat capacity values of PEEK polymer from the Athas database.[71] Among the different heating rates, the neat PEEK results at 5 K/min exhibited the closest agreement with the Athas database values.[71] The ROM results, obtained using dry carbon fiber heat capacities with 10 K/min heating rate, reveal a sudden increase in Cp values between 65 and 140 °C, a phenomenon absent in the other two cases. Furthermore, from 50 °C to the glass transition region, the composite heat capacities from the available literature consistently surpass the values obtained from the rule of mixture. The values from the open literature were selected based on their trustworthiness, which includes proper documentation of measurement procedures, applied standards, and techniques. As a result, these sources [28][31][47] were deemed to be the most reliable data. Beyond the glass transition region, the results of the ROM using the carbon fiber heat capacities at 20 K/min coincide well with the literature values, while in the other cases the ROM resulted in higher specific heats. It is interesting to note that in the case of dry carbon fibers the decrease in heating rate did not increase the resultant Cps shown in Figure 32, as was the case with the neat PEEK and composite samples, in fact that exact opposite trend can be observed.

Figure 22 shows the coefficient of variation of the heat capacity measurements for pure carbon fibers under various heating rates. Additionally, it presents the coefficient of variation for neat PEEK heat capacities at a 5 K/min heating rate. Figure 23 shows the coefficient of variation of the rule of mixture results. Figure 22 highlights the considerable variation in the obtained heat capacity results for pure carbon fibers. At a 20 K/min heating rate, the variability ranges from 16 % to 45 %, while using 10 K/min heating rate this variation falls within 15 - 36 %, showcasing a slight decrease. For neat PEEK results at a 5 K/min heating rate, the variability changes between 2% and 4 % from 40 °C to 300 °C, gradually increasing to 6 % above 300 °C.

The standard deviations for ROM results were calculated using the formula for error propagation and then divided by their corresponding mean values to obtain the coefficients of variation. As expected, the pronounced variation in the pure carbon fiber measurements is inherited over to the variation of the ROM of mixture results as well. Using the CF heat capacities with a 20 K/min heating rate, the ROM exhibits variability between 10 % and 22 %. For ROM obtained with CF heat capacities at a 10 K/min rate, the variation ranges from 8 % to 18 %, while using CF heat capacities at a 5 K/min rate yields a resultant ROM variability of around 7 %.

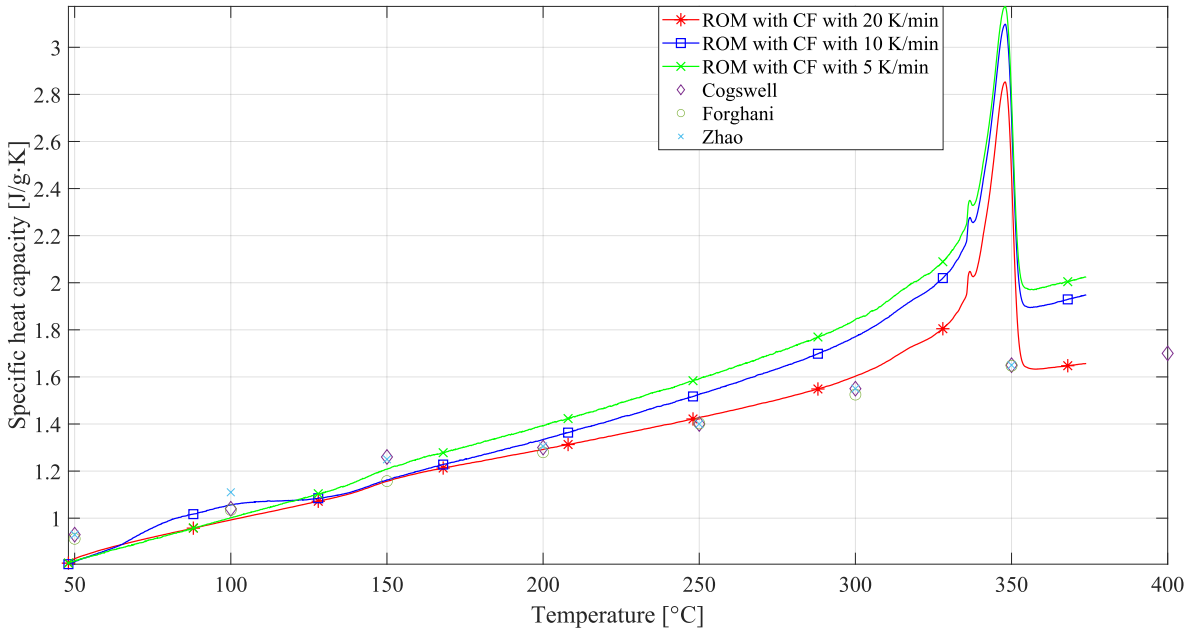

Figure 21: Calculated specific heats using the rule of mixtures

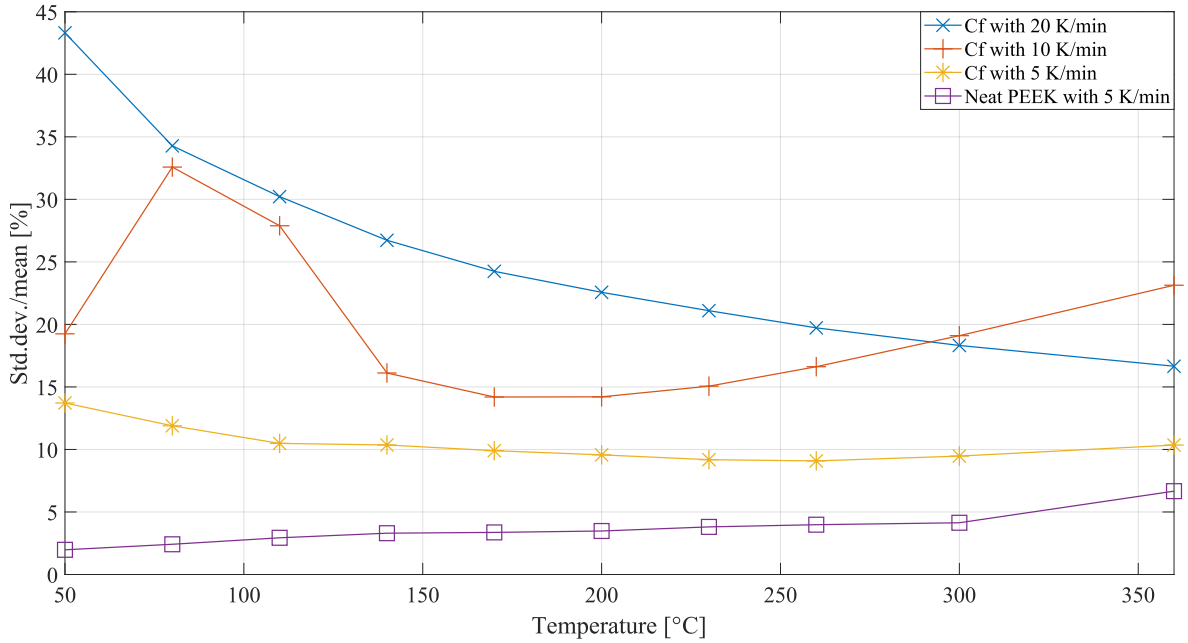

Figure 22: Coefficient of variation of the dry carbon fibers and the neat PEEK granulates

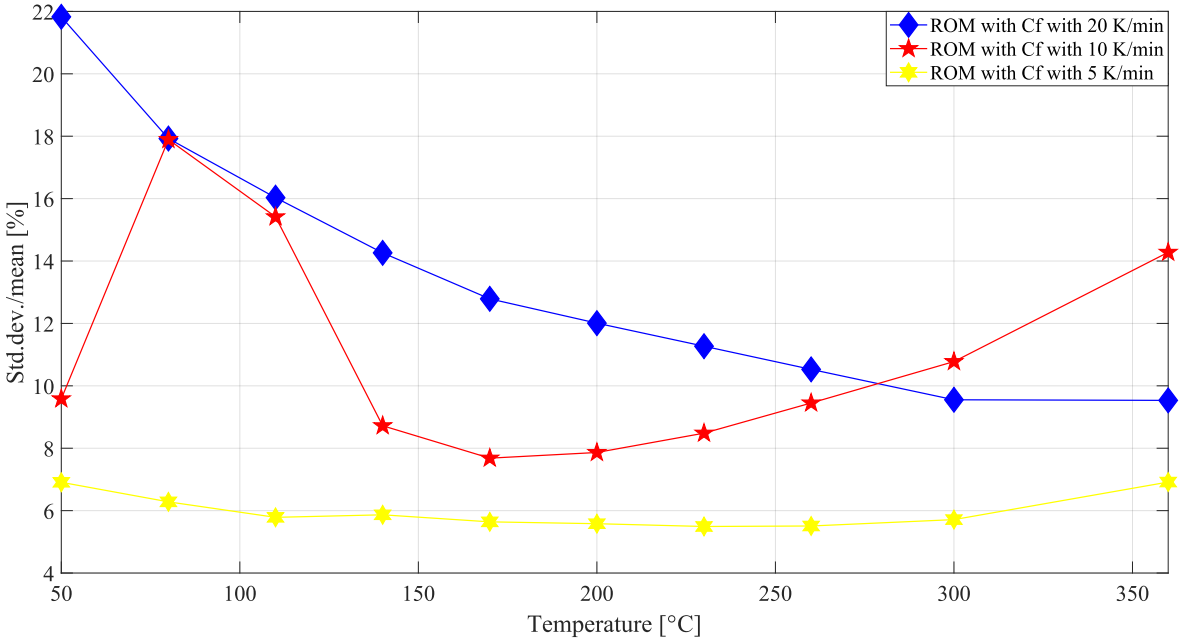

Figure 23: Coefficient of variation using the ROM

5.6 Comparing the results to literature

As it was mentioned in subsection 5.4 the specific heat capacities obtained in the case of 4ply samples with 10 and 5 K/min heating rate as well as the heat capacity of 7ply samples with 5 K/min heating rate resulted in the best matches with the highest obtained heat capacities. Figure 24 shows the heat capacity results of the 4-ply samples with 10 K/min heating rate, alongside with three temperature-dependent heat capacities from the literature, which are the same as presented in subsection 5.5. If one compares the specific heat capacities obtained upon cooling a nice agreement can be seen between the values from literature and the measured heat capacities. It is interesting to note that the specific heat capacities obtained upon heating are consistently higher than the results upon cooling and the data from the literature. This phenomenon only manifested itself in the case of composite samples. This was not encountered in the measurements of the neat PEEK samples. This phenomena was traced back to the asymmetry of the baselines upon heating and cooling. Figure 24b shows the heat capacity results of the 4ply samples with 10 K/min heating rate obtained with the mirrored baseline upon cooling. This means that the measured baseline upon cooling is multiplied by minus one to be applicable for the calculation of the specific heat capacity upon heating, or in other words it was mirrored with respect to the 'x' axis. In this case the heating and cooling heat capacities coincide well with each other as well as with the literature values. This finding shows that reliable heat capacity values can be obtained with different samples, if the proper measurement conditions are applied. The comparison of the 4ply samples with 5 K/min heating rate and the 7ply samples with 5 K/min heating rate with the literature values and their result using the mirrored cooling baselines can be found in subsection A.7.

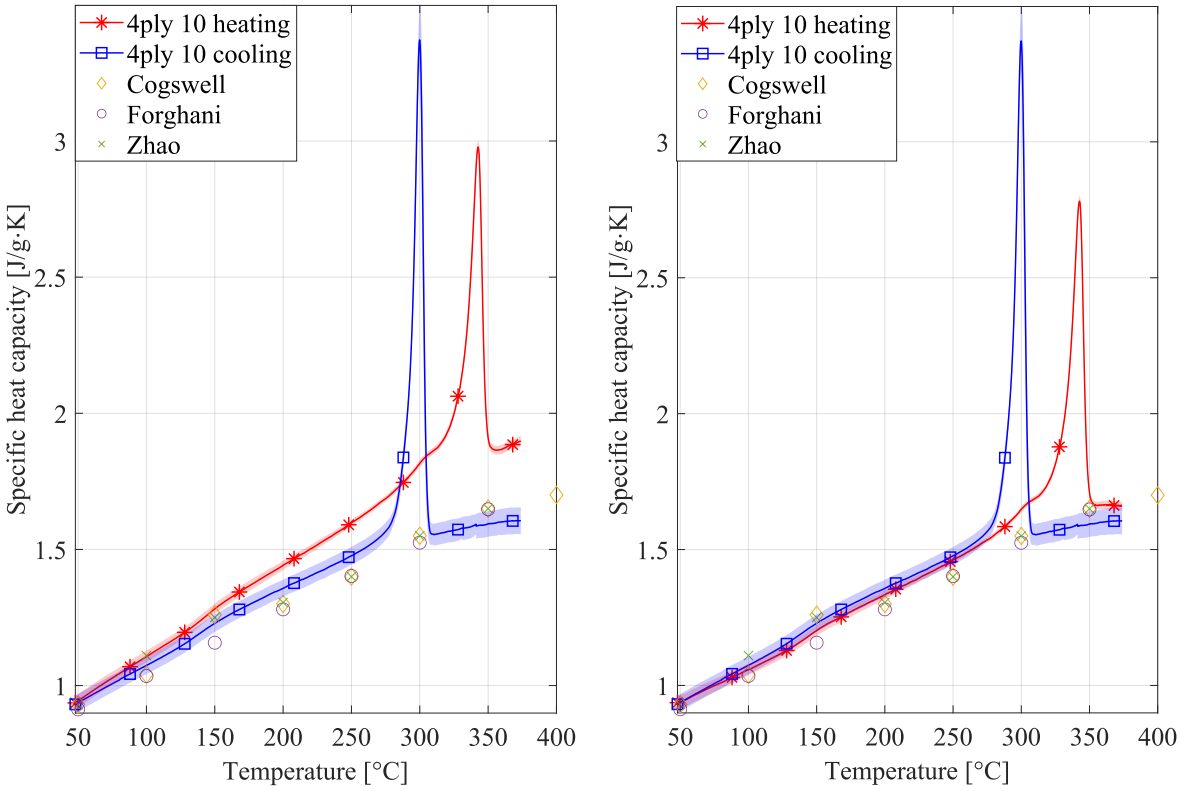

(a) Cp of the 4ply samples with 10 K/min heating rate

(b) Cp of the 4ply samples using mirrored the cooling baseline

Figure 24: Comparison of the measured specific heat capacities to literature

5.7 Uncertainties during DSC experiments

According to the ASTM E1269 [34], when describing the measurement uncertainty three terms must be evaluated, namely the measurement repeatability, reproducibility and bias.

The measurement repeatability is defined as the closeness of subsequent measurements completed with the same material under identical measurement conditions. Therefore, the applied temperature program, heating rate, sample and crucibles have to be the same in all cases. This was evaluated on the measurements of sapphire disk as the reference material for heat capacity determination. The repeatability was calculated by multiplying the relative standard deviation by 2.8, resulting in a repeatability value within 95 % confidence limit. This assessment was performed at each applied heating rate of 5, 10, and 20 K/min. In the case of 20 K/min heating rate, six sapphire measurements were conducted, while in the cases of 10 and 5 K/min heating rate, 4 measurements were carried out. The results are shown in Table 12.

The reproducibility of the heat capacity measurements was determined as the closeness of the measurement results, when the measurement conditions have changed. In this case, the heat capacities of the sapphire standard with different heating rates were evaluated in order to assess the reproducibility of the results with varied measurement

conditions. This was achieved by multiplying the relative standard deviations by 2.8.

Lastly, the bias of the measurement has also been determined. The bias, in this context, refers to the deviation of the obtained results for a well-known substance from its literature value. This evaluation was conducted on the sapphire reference, given its well-defined and accurately measured heat capacity over a wide temperature range.

According to the ASTM standard [34], a repeatability of 6.2 % was obtained in an interlaboratory study. As can be seen from Table 12, the repeatabilities obtained with 20 and 5 K/min heating rates resulted in values with close agreement, only in the case of 10 K/min heating rate yielded higher repeatabilities, between 10 and 11 %. Therefore, being less repeatable.

Regarding the reproducibility of the results, the standard states that a reproducibility of 8.4 % was achieved in this above mentioned interlaboratory study, which coincides well with the values obtained in this study.

Lastly, the bias of the measurement was stated to be between -1.1 % and 1.8 % depending on the material that was used, as well as on the reference values from literature that the results were compared to. In this study a bias between - 2.3 and 3.4 % were obtained according to the different heating rates shown in Table 13.

Table 12: Repeatability and reproducibility of the measurements

Temp. [°C]	**Repeatability with 20 K/min [%]**	**Repeatability with 10 K/min [%]**	**Repeatability with 5 K/min [%]**	**Reproducibility [%]**
100	5.32	10.89	5.15	9.9
200	5.68	10.07	4.95	8.81
300	5.05	11.14	6.2	8.22

Table 13: Bias of the measurements

Temp. [°C]	**Bias for 20k/min [%]**	**Bias for 10k/min [%]**	**Bias for 5 k/min [%]**	**Sapphire Cp from lit. [34] [J/gK]**
100	-2.25	1.27	3.31	0.9071
200	-2.01	1.2	2.95	1.0291
300	-1.57	1.35	3.39	1.0895

6 Discussion

6.1 Influence of baseline and sample types

From the results of the baseline consistency and from influence of the sample mass, shape and form shown in subsection 5.1 and subsection 5.2 respectively, it can be concluded that samples with higher weights such as the 4ply and 7ply samples are favorable for heat capacity determination. First of all, they are less susceptible to baseline deviations due to their higher heat flow rate. Their signal-to noise ratio is also better than of the lighter samples. Therefore, making it easier to detect and measure the heat capacity accurately. Moreover, heavier samples showcased lower variability as was shown in Figure 13, resulting in more consistent results. These finding align with the observations made by other authors when measuring the specific heat of various materials. Fernandes et al.[72] observed a notable decrease in variability in the capacity values when sapphire samples with higher weight were tested. Moreover, Gilmour and Hay [73], investigated the influence of sample mass on the specific heat of polystyrene among others. They also noted an increase in specific heat with higher sample weights up to a certain weight, after which the heat capacity started to decrease with further increases in weight. They attributed this phenomenon to the accumulation of temperature gradients within the samples with higher weights.

The shape of the samples had a much less influence on the resultant specific heat capacities. From the results shown in Figure 14, it can be concluded that it is more important to have sufficient mass and to achieve good thermal contact between the samples and crucible than the shape of the sample, which is supported by the close agreement of the 7ply disk and 7ply unordered samples specific heat capacities. However, for accurate measurement the disk shaped specimens were preferred as they showcased lower variability in their results.

Regarding the sample form, the powder samples consistently yielded similar heat capacity values compared to the layered specimens. However, the accuracy of these measurements were noticeably lower indicated by their higher variability. This could be partly attributed to the air voids present in the powder samples. The milling of laminate surfaces resulted in relatively large chunks of composite particles. Therefore, when loading them into the pan, air pockets unavoidably remained between the powder particles, despite the efforts to compress the powder in the pan using a rod as much as possible, hindering the efficient heat transfer. Moreover, the pan-specimen contact interface is likely less well established with the powder samples than of the disk-shaped samples. In the work of Ramakumar et al.[74], the authors compared the specific heat capacities of sapphire using a disk shaped samples and high purity powder. They reported the same trend as in this study, which is that powder samples gave similar values as the disk-shaped specimens, however the spread of the results were notably higher in the case powder samples. The authors attributed this phenomenon solely to the to the better thermal contact achieved with the disk shaped samples. Consequently, this type of sample preparation did not live up to its expectation. A more effective approach could involve grinding the composite sample into much finer powder particles to minimize the presence of air voids. However, it may not be justified to invest substantial

effort into preparing finely powdered samples for heat capacity measurements when reliable results can be obtained with layered specimens, necessitating significantly less processing.

To sum it up, samples with higher masses are recommended for accurate heat capacity determination, which in this study was the 4ply samples and 7ply samples with average weight of 17.35 mg and 28.29 mg respectively. The sample shape and form had lesser influence on the resultant heat capacities, but had more impact on the variability of the results. Therefore, for the sake of thriving for more accurate measurement it is advised to make solid samples resembling the shape of the crucible in order to maximize the surface contact between the samples and crucibles and to avoid air pockets within the samples.

6.2 Influence of the thermal cycles

As it was mentioned in subsection 5.3, the 1ply samples had undergone kinetic events such as the sharp glass transition and cold crystallization in the first cycle, which were absent in the second cycle. This phenomenon can be attributed to the manufacturing of the carbon fiber tapes, whereas the tapes go through a rapid cooling process (quenched state), which does not allow sufficient time for the polymer to crystallize. This is then achieved in the first thermal cycle. These above mentioned kinetic phenomenon has been observed by other researchers as well.[47] It was also observed that these kinetic events did not occur in the case of the layered samples. This could be attributed to the consolidation process, that the layered samples underwent before the heat capacity measurement. It is plausible, that these samples may have already experienced these kinetic events upon consolidation, considering they are derived from the as-received unidirectional tapes.

It was observed, that the layered samples exhibited a double melting peak in the first heat up cycle shown in Figure 17. According to Blundell et. al.[75], there are two main theories aiming to explain this phenomena. The first theory indicates, that the observed phenomenon is the result of continuous melting and recrystallization of the PEEK matrix. The first shallow peak indicates the onset of the melting of the crystals, while the region between the two melt peaks is where the molecules undergo a continuous process of melting and recrystallization. The second melt peak can interpreted as the point where net difference between melting and recrystallization reaches its maximum point. In contrast to that, the second theory detailed by Blundell et. al.[75] explains the double melt peak with the formation of different crystal populations. Besides the main crystal formation, less stable crystals are also formed within the voids between the main crystals and the subsequent melting of those less stable crystals are responsible for the first shallow melt peak, while the melting of the main crystals cause the sharp second melt peak. Consequently, competing theories exist in the open literature aiming to explain the double melt peak phenomenon, underlining the ongoing debate on the exact governing mechanism.

Regrading the crystallinity content between the two heat up cycles, only a slight variation was observed in the case of the layered samples, while the as-received 1ply samples exhibited a substantial increase in crystallinity during the first heat up cycle. As a result, one would expect the specific heat of the second cycle to be lower than of the first cycle due to the increased crystalline content, since the crystalline portion of the PEEK matrix has a lower heat capacity compared to its amorphous counterpart according to Varma-Nairet et. al.[76]. However, by looking at Figure 16 one could see that this is not case, in fact the exact opposite trend can be observed. It is possible, that the initially wavy nature of the as-received tapes results in suboptimal contact with the crucible. Moreover, as the samples heat up, they warp which can further decrease the goodness of the contact. This situation may be improved upon the first melting, as the gravitational force helps draw down the molten composite, facilitating better contact with the pan, which in turn can significantly improve the heat transfer between the samples and the crucibles resulting in higher heat capacities. The achievement of better thermal contact between the samples and the pans upon melting occurs to the 4ply and 7ply samples, albeit with a lesser effect, as these samples had undergone press consolidation, which generally results in flatter specimens. Consequently, the influence of melting and gravitational forces in improving contact is less pronounced in these cases. Moreover, the slight change in polymer microstructure (decreased crystallinity) may also attribute to the small increase in heat capacities observed during the second cycle, however the discrepancy is so little between the degree of crystallinity in the first and second cycle that it might as well be negligible.

Last but not least, the measured temperature range in this study was set between 40 °C and 380 °C in order to provide heat capacity data over a wide temperature range. Selecting proper temperature limits is crucial in order to avoid the effects arising from the degradation of the samples. These effects can be rather severe as thermal degradation can cause chain scission, which leads to the decrease in molecular weight or in severe cases to char formation as was shown in the work of Patel et al.[77]. These irreversible structural changes in the polymer can significantly alter its thermal properties including the specific heat capacity. Moreover, exposing the composite samples to elevated temperatures can lead to significant weight loss. According to the ASTM standard [34], a weight loss exceeding 0.3 % of the initial sample weight renders the measurement invalid.

To sum it up, the inherent thermal history can have a significant effect on the resultant specific heat capacities especially in the case of unprocessed samples. Therefore, it is advisable to apply two subsequent and identical thermal cycles. Firstly, the application of two thermal cycles erases the initial thermal history of the samples. Secondly, it introduces a new controlled thermal history, which is the same for all samples, allowing meaningful comparisons from the second thermal cycle. The temperature limits of the thermal cycles should be selected carefully to avoid thermal degradation. Last but not least, specific heat capacity from the first thermal cycle can be of use for comparing, as well as for obtaining information on the influence of different manufacturing processes on the composites thermal behaviours.

6.3 Influence of the heating rate

Regarding the influence of the applied heating rate that was detailed in subsection 5.4, it is evident that a working range exists in the choice of heating rates and sample mass. This working range balances the need for sufficient heat flow into the samples, which reduces susceptibility to baseline deviations, as sample weight increases, so does heat flow. Moreover, it fulfills the desire for higher heating rates to expedite the measurements. All while preventing the build-up of thermal gradients within the samples, which as shown in subsection 5.4 can have a significant influence on the results. In this study, this optimal compromise is found with the 4ply samples using 10 K/min heating rate. This choice effectively eliminates the need for the slower 5 K/min heating rate required for the 7ply samples, substantially speeding up the measurement process, while still yielding heat capacity results in close agreement, within 5 % deviation.

6.4 Rule of mixtures

As mentioned in the results of the rule of mixtures in subsection 5.5, a sudden increase in the heat capacity values using the results of the pure CF with 10 K/min heating rate was observed between 65 °C and 140 °C. This phenomenon was traced back to the heat capacity measurement of pure carbon fibers where this exact same trend was observed. This can be attributed to the insufficient and constantly changing contact between the crucibles and the pure carbon fibers, because the dry carbon fibers resemble closely the human hair. Therefore, it was rather challenging to cut the fibers to similar sizes as the small crucibles. Moreover, it is almost impossible to press them down to the bottom of the crucible and to ensure that the fibers remain there, since they visibly sprang back during preparation. This problem clearly manifests itself when examining the standard deviations of the pure carbon fiber results, which are considerably higher than those of the composite or the neat PEEK as shown in Figure 23. Consequently, while it was possible to obtain similar heat capacity results using the ROM as the direct measurement of the heat capacity of the composite. However, the preparation of the pure carbon fiber samples, including the burn-off process to expose the carbon fibers and then preparing them for DSC measurement, required significantly more time and effort than just using composite samples. Moreover, the very high standard deviations indicate a significant spread in the results when using this approach to obtain composite specific heats, notably higher than that of the composite samples with proper measurement conditions. In conclusion, the mixture rule can be used for Cp determination. However, the problematic heat capacity measurement of pure carbon fibers makes this approach rather impractical due to its cumbersomeness and inaccuracy.

6.5 Comparing of the measured heat capacities to literature

In subsection 5.6, it was noted that the obtained heat capacities regrading the composite samples differ upon heating and cooling. However, in theory the heat capacity of the materials should be the same regardless if the material heats up or cools down. The

root cause of this unexpected phenomenon was traced back to the baseline-corrected heat flows of the samples, the actual measurement signal obtained on the DSC machine. These heat flows exhibited a similar deviation as the resultant specific heat capacities. It means, that the samples absorbed more heat upon heating, than released upon cooling, which in turn resulted in the deviation between the heating and cooling heat capacities. This phenomenon only manifested itself in the case of composite samples with lower heating rates. By mirror the baselines upon cooling and using it for the heat capacity determination effectively mitigated this discrepancy. This phenomena was not encountered in the measurements of the neat PEEK samples. Therefore, it may be attributed to the structure of the composite samples. However, further investigation would be needed to find the underlying cause of this phenomenon.

6.6 Proposed guidelines

Based on the carried out experiments and from the observations the following guidelines and best practices were formulated for heat capacity measurements of thermoplastic composites:

- Performing baseline measurements frequently in order to check their consistency, and if any notable shift is observed, action can be taken.
- Use the mass of at least 15 [mg] to reduce the susceptibility to baseline deviations and to obtain results with low variability.
- Use of unidirectional or cross ply layups can be both utilized.
- It is advised to use disk shaped specimen. However, it does not have a significant impact on the results if good thermal contact is achieved between the samples and crucibles.
- Use heating rate between 10 and 5 K/min in order to avoid the accumulation of significant temperature gradients within the samples.
- Employ two thermal cycles in order to get rid of the inherent thermal history of the samples and to introduce one which is the same for all specimens, allowing meaningful comparisons.
- Obtain the specific heat capacities from the second cycle.
- Use of at least 10 minute equilibrium between each dynamic segment in order to allow the samples to reach equilibrium before starting a new segment.
- Careful choice of the maximum applied temperature in order to avoid thermal degradation of the samples (material dependent).

7 Conclusion and recommendations

In this study, the significance of obtaining precise heat capacity values for composites was discussed. The absence of measurement guidelines for heat capacity determination regarding the composites were highlighted. The most commonly used method for characterizing an unknown substance specific heat capacity is differential scanning calorimetry. The operational principles of the DSC machine and the method for determining heat capacity were examined in detail. A comprehensive literature review was provided, delving into the previous attempts to measure the specific heat capacity of composites, including the general guidelines of the DSC manufacturers for accurate heat capacity determination. Experimental investigations were conducted to explore the influence of sample preparations, such as weight, shape, and form. Additionally, the impact of various measurement parameters, including the temperature program and heating rate, were assessed. The significance of frequent baseline measurements was underscored. Moreover, the impact of temperature gradients within the samples have been discussed as well. Therefore, the formulated research questions, can be found in subsection 1.5, have been addressed. The collective findings from these experiments led to the establishment of guidelines and best practices for measuring the specific heat capacity of composites through the utilization of differential scanning calorimetry. The outcomes presented herein contribute to the evolving methodologies in the field and serving as a step forward for standardized heat capacity measurements for composite materials.

7.1 Recommendations

The next step towards standardizing specific heat capacity measurements of composites involves extending the investigation to other relevant composites with thermoplastic matrices, including but not limited to PEI, PPS, PEKK, or Victrex LM-PAEK. This expansion would provide a comprehensive dataset for researchers. Moreover, it would help facilitating the assessment of various influential parameters during measurements with different material combinations. Furthermore, the characterization of thermoplastic composites with different reinforcement such as glass or aramid fibers has not been addressed adequately to date. Additionally, exploring the influence of different fiber arrangements, such as woven fibers and other types of fabrics, also remains an area that requires further investigation.

In terms of measurement conditions, testing smaller increments of heating rates over a wider range would be beneficial for further optimization of the heat capacity determination for specific composites. This approach would help eliminate uncertainty arising from temperature gradients in the samples. Additionally, it is essential to explore limiting temperatures for different thermoplastic matrices and fiber types to obtain reliable results, while avoiding thermal degradation and and other unwanted phenomena.

Furthermore, the observed deviation between the heat capacities obtained upon heating and cooling at decreasing heating rates needs to be investigated in more detail to determine whether it arises from a measurement artifact or is inherent to the nature of composite materials.

Additionally, temperature-modulated DSC (TM-DSC) measurements could be conducted. This technique utilizes the same apparatus as a conventional DSC, employing a linear heating ramp, but also superimposes a sinusoidal signal on this linear ramp. This results in the constant temperature increase of the samples as well. However, this increase is not linear but sinusoidal. TM-DSC allows researchers to determine the specific heat capacity of unknown samples with just one measurement (excluding the calibration run), significantly expediting the process. Moreover, this technique is less reliant on baseline stability compared to the three-run method in conventional DSC measurements, addressing the crucial need for a stable baseline throughout the measurement sequence. Additionally, the thermal history of the samples poses less of an issue, as TM-DSC can effectively distinguish changes in heat flows caused by heat capacity from those induced by kinetic events such as cold crystallization or melting.

8 References

References

[1] Anthony R. Bunsell, Sébastien Joannès, and Alain Thionnet. *Fundamentals of Fibre Reinforced Composite Materials*. Feb. 2021. DOI: 10.1201/9780429399909. URL: https://doi.org/10.1201/9780429399909.

[2] Jing Zhang. "Different surface treatments of carbon fibers and their influence on the interfacial properties of carbon fiber/epoxy composites". In: (Sept. 2012).

[3] Jitha S. Jayan et al. *An introduction to fiber reinforced composite materials*. Jan. 2021, pp. 1–24. DOI: 10.1016/b978-0-12-821090-1.00025-9. URL: https://doi.org/10.1016/b978-0-12-821090-1.00025-9.

[4] J. Bijwe S. Tiwari. "Surface Treatment of Carbon Fibers - A Review". In: *Procedia Technology* 14.1 (2014), pp. 505–512.

[5] Victor Giurgiutiu. "Chapter 1 - Introduction". In: *Structural Health Monitoring of Aerospace Composites*. Ed. by Victor Giurgiutiu. Oxford: Academic Press, 2016, pp. 1–23. ISBN: 978-0-12-409605-9. DOI: https://doi.org/10.1016/B978-0-12-409605-9.00001-5. URL: https://www.sciencedirect.com/science/article/pii/B9780124096059000015.

[6] Avery Thompson. "Why the 787 Dreamliner's Windows Are So Big". In: (Nov. 2017). URL: https://www.popularmechanics.com/flight/a25052/why-the-dreamliners-windows-so-big/.

[7] S.J. Pickering. "Recycling technologies for thermoset composite materials—current status". In: *Composites Part A: Applied Science and Manufacturing* 37.8 (2006). The 2nd International Conference: Advanced Polymer Composites for Structural Applications in Construction, pp. 1206–1215. ISSN: 1359-835X. DOI: https://doi.org/10.1016/j.compositesa.2005.05.030. URL: https://www.sciencedirect.com/science/article/pii/S1359835X05002101.

[8] Robynne E. Murray et al. "Structural validation of a thermoplastic composite wind turbine blade with comparison to a thermoset composite blade". In: *Renewable Energy* 164 (2021), pp. 1100–1107. ISSN: 0960-1481. DOI: https://doi.org/10.1016/j.renene.2020.10.040. URL: https://www.sciencedirect.com/science/article/pii/S0960148120316062.

[9] B. Sarh W. G. Roeseler and M.U. Kismarton. "Composite structures: The first 100 years." In: *ICCM International Conferences on Composite Materials*. 2007.

[10] Ginger Gardiner. "Thermoplastic composites: Primary structure?" In: (July 2019). URL: https://www.compositesworld.com/articles/thermoplastic-composites-primary-structure.

[11] Robert R. Brooks et al. “A review on stamp forming of continuous fibre-reinforced thermoplastics”. In: *International Journal of Lightweight Materials and Manufacture* 5.3 (May 2022), pp. 411–430. DOI: 10.1016/j.ijlmm.2022.05.001. URL: https://doi.org/10.1016/j.ijlmm.2022.05.001.

[12] Uday K. Vaidya and K. K. Chawla. “Processing of fibre reinforced thermoplastic composites”. In: *International Materials Reviews* 53.4 (July 2008), pp. 185–218. DOI: 10.1179/174328008x325223. URL: https://doi.org/10.1179/174328008x325223.

[13] Fazil O. Sonmez and Mustafa Akbulut. “Process optimization of tape placement for thermoplastic composites”. In: *Composites Part A-applied Science and Manufacturing* 38.9 (Sept. 2007), pp. 2013–2023. DOI: 10.1016/j.compositesa.2007.05.003. URL: https://doi.org/10.1016/j.compositesa.2007.05.003.

[14] Ginger Gardiner. “Consolidating thermoplastic composite aerostructures in place, Part 1”. In: (June 2020). URL: https://www.compositesworld.com/articles/consolidating-thermoplastic-composite-aerostructures-in-place-part-1.

[15] Ali Yousefpour, Mehdi Hojjati, and Jean-Pierre Immarigeon. “Fusion Bonding/Welding of Thermoplastic Composites”. In: *Journal of Thermoplastic Composite Materials* 17.4 (2004), pp. 303–341. DOI: 10.1177/0892705704045187. eprint: https://doi.org/10.1177/0892705704045187. URL: https://doi.org/10.1177/0892705704045187.

[16] Zhenhai Guo and Xudong Shi. *Temperature–Time Curve of Fire and the Equation of Heat Conduction*. Jan. 2011, pp. 76–90. DOI: 10.1016/b978-0-12-386962-3.10005-1. URL: https://doi.org/10.1016/b978-0-12-386962-3.10005-1.

[17] Manuel Längauer et al. “Enhanced Simulation of Infrared Heating of Thermoplastic Composites Prior to Forming under Consideration of Anisotropic Thermal Conductivity and Deconsolidation by Means of Novel Physical Material Models”. In: *Polymers* 14.16 (Aug. 2022), p. 3331. DOI: 10.3390/polym14163331. URL: https://doi.org/10.3390/polym14163331.

[18] João Carlos R. Reis, M.F.S.F. De Moura, and Sylwester Samborski. “Thermoplastic Composites and Their Promising Applications in Joining and Repair Composites Structures: A Review”. In: *Materials* 13.24 (Dec. 2020), p. 5832. DOI: 10.3390/ma13245832. URL: https://doi.org/10.3390/ma13245832.

[19] Rex J. Kuriger et al. “Processing and characterization of aligned vapor grown carbon fiber reinforced polypropylene”. In: *Composites Part A-applied Science and Manufacturing* 33.1 (Jan. 2002), pp. 53–62. DOI: 10.1016/s1359-835x(01)00070-7. URL: https://doi.org/10.1016/s1359-835x(01)00070-7.

[20] Lisa Rivière et al. “Specific heat capacity and thermal conductivity of PEEK/Ag nanoparticles composites determined by Modulated-Temperature Differential Scanning Calorimetry”. In: *Polymer Degradation and Stability* 127 (May 2016), pp. 98–104. DOI: 10.1016/j.polymdegradstab.2015.11.015. URL: https://doi.org/10.1016/j.polymdegradstab.2015.11.015.

[21] Mariaenrica Frigione et al. “Modeling of continuous ultrasonic impregnation and consolidation of thermoplastic matrix composites”. In: *Composites Part A-applied Science and Manufacturing* 82 (Mar. 2016), pp. 119–129. DOI: 10.1016/j.compositesa.2015.12.004. URL: https://doi.org/10.1016/j.compositesa.2015.12.004.

[22] R. Phillips et al. “Influence of processing parameters on the dimensional stability of polymer composites”. In: 1994, pp. 167–174. URL: http://infoscience.epfl.ch/record/179113.

[23] Agust ´ Õn Salazar. “On thermal diffusivity”. In: *European Journal of Physics* 24.4 (May 2003), pp. 351–358. DOI: 10.1088/0143-0807/24/4/353. URL: https://doi.org/10.1088/0143-0807/24/4/353.

[24] Bernard Budiansky. “Thermal and Thermoelastic Properties of Isotropic Composites”. In: *Journal of Composite Materials* 4.3 (July 1970), pp. 286–295. DOI: 10.1177/002199837000400301. URL: https://doi.org/10.1177/002199837000400301.

[25] Carlos E. S. Bernardes, Abhinav Joseph, and Manuel E. Minas Da Piedade. “Some practical aspects of heat capacity determination by differential scanning calorimetry”. In: *Thermochimica Acta* 687 (May 2020), p. 178574. DOI: 10.1016/j.tca.2020.178574. URL: https://doi.org/10.1016/j.tca.2020.178574.

[26] Shamala Sambasivam. “Thermoelastic stress analysis of laminated composite materials”. PhD thesis. University of Southampton, Oct. 2009. URL: https://eprints.soton.ac.uk/72144/.

[27] Hector H. Garcia. “Modeling Fire Behavior of a Carbon Fiber Reinforced Polyimide Composite”. In: *Luleå University of Technology Department of Engineering Sciences and Matematics* (Jan. 2015). URL: http://www.diva-portal.org/smash/record.jsf?pid=diva2:1020615.

[28] “Appendix 8 - Thermophysical properties of carbon fibre reinforced polyetheretherketone containing 61% by volume of high strength carbon fibre”. In: *Thermoplastic Aromatic Polymer Composites*. Ed. by Frederic Neil Cogswell. Butterworth-Heinemann, 1992, p. 241. ISBN: 978-0-7506-1086-5. DOI: https://doi.org/10.1016/B978-0-7506-1086-5.50026-4. URL: https://www.sciencedirect.com/science/article/pii/B9780750610865500264.

[29] Dennis Maurer and Peter Mitschang. “Laser-powered tape placement process – simulation and optimization”. In: *Advanced manufacturing* 1.3 (Nov. 2015), pp. 129–137. DOI: 10.1080/20550340.2015.1114798. URL: https://doi.org/10.1080/20550340.2015.1114798.

[30] Omar Baho et al. “Simulation of laser heating distribution for a thermoplastic composite: effects of AFP head parameters”. In: *The International Journal of Advanced Manufacturing Technology* 110.7-8 (Sept. 2020), pp. 2105–2117. DOI: 10.1007/s00170-020-05876-9. URL: https://doi.org/10.1007/s00170-020-05876-9.

[31] Fanfan Zhao et al. "The effect of temperature field on the characteristics of carbon fiber reinforced thermoplastic composites in the laying and shaping process". In: *The International Journal of Advanced Manufacturing Technology* 121.11-12 (Aug. 2022), pp. 7569–7589. DOI: 10.1007/s00170-022-09795-9. URL: https://doi.org/10.1007/s00170-022-09795-9.

[32] Po-Jen Shih. "On-line consolidation of thermoplastic composites". In: *ResearchGate* (Jan. 1997). URL: https://www.researchgate.net/publication/237711561_On-line_consolidation_of_thermoplastic_composites.

[33] John Tierney and John W. Gillespie. "Modeling of Heat Transfer and Void Dynamics for the Thermoplastic Composite Tow-Placement Process". In: *Journal of Composite Materials* 37.19 (Oct. 2003), pp. 1745–1768. DOI: 10.1177/002199803035188. URL: https://doi.org/10.1177/002199803035188.

[34] "Test Method for Determining Specific Heat Capacity by Differential Scanning Calorimetry". In: *American Society for Testing and Materials (ASTM)* (May 2018). DOI: 10.1520/e1269-11r18. URL: https://doi.org/10.1520/e1269-11r18.

[35] Wikipedia contributors. *Joseph Black*. Mar. 2023. URL: https://en.wikipedia.org/wiki/Joseph_Black.

[36] Jr. Darryl Baker. *Thermal Characterization Of Carbon Composites*. 2011. URL: https://digital.library.ncat.edu/theses/13.

[37] Nicholas P. Cheremisinoff. *THERMAL ANALYSIS*. Jan. 1996, pp. 17–24. DOI: 10.1016/b978-081551403-9.50004-2. URL: https://doi.org/10.1016/b978-081551403-9.50004-2.

[38] Roger L. Blaine. *THE CASE FOR A GENERIC DEFINITION OF DIFFERENTIAL SCANNING CALORIMETRY*. 2013. URL: https://www.tainstruments.com/pdf/literature/TA081.pdf.

[39] G. Dallas, J. Groh, and T. Kelly. *Improved DSC Performance Using Tzero™ Technology*. 2001. URL: https://www.tainstruments.com/pdf/literature/tzero.pdf.

[40] TA Instruments. *Differential Scanning Calorimetry (DSC) Practical Training Course*. 2020. URL: https://www.tainstruments.com/wp-content/uploads/Discovery_DSC_practical_2020_part_1.pdf.

[41] Louis Waguespack and Roger Blaine. *Design of a New DSC Cell with Tzero Technology*. 2001. URL: https://www.tainstruments.com/pdf/literature/TA273.pdf.

[42] "Plastics — Differential scanning calorimetry (DSC) — Part 4: Determination of specific heat capacity". In: *International Organization for Standardization (ISO)* (June 2014). URL: https://www.iso.org/standard/65087.html.

[43] Andrew A. Johnston. *An integrated model of the development of process-induced deformation in autoclave processing of composite structures*. DOI: 10.14288/1.0088805.

[44] Georgios Kalogiannakis, Danny Van Hemelrijck, and Guy Van Assche. "Measurements of Thermal Properties of Carbon/Epoxy and Glass/Epoxy using Modulated Temperature Differential Scanning Calorimetry". In: *Journal of Composite Materials* 38.2 (Jan. 2004), pp. 163–175. DOI: 10.1177/0021998304038647. URL: https://doi.org/10.1177/0021998304038647.

[45] Volkan Cecen et al. "Epoxy- and polyester-based composites reinforced with glass, carbon and aramid fabrics: Measurement of heat capacity and thermal conductivity of composites by differential scanning calorimetry". In: *Polymer Composites* 30.9 (Sept. 2008), pp. 1299–1311. DOI: 10.1002/pc.20695. URL: https://doi.org/10.1002/pc.20695.

[46] Muhammad Amir Khan. "Experimental and Simulative Description of the Thermoplastic Tape Placement Process with Online Consolidation". doctoralthesis. Technische Universität Kaiserslautern, 2017, pp. XII, 126. URL: http://nbn-resolving.de/urn:nbn:de:hbz:386-kluedo-47293.

[47] Erfan Forghani. "Effect of temperature dependence of PEEK composite material properties in modelling resistive welding". PhD thesis. University of British Columbia, 2022. DOI: http://dx.doi.org/10.14288/1.0418599. URL: https://open.library.ubc.ca/collections/ubctheses/24/items/1.0418599.

[48] A Kollmannsberger et al. "Numerical analysis of the temperature profile during the laser-assisted automated fiber placement of CFRP tapes with thermoplastic matrix". In: *Journal of Thermoplastic Composite Materials* 31.12 (Nov. 2017), pp. 1563–1586. DOI: 10.1177/0892705717738304. URL: https://doi.org/10.1177/0892705717738304.

[49] Kishore Kumar Mahato, Krishna Dutta, and Bankim Chandra Ray. *Emerging advancement of fiber-reinforced polymer composites in structural applications*. Jan. 2020, pp. 221–271. DOI: 10.1016/b978-0-12-818961-0.00006-5. URL: https://doi.org/10.1016/b978-0-12-818961-0.00006-5.

[50] D J Blundell and B N Osborn. "Crystalline morphology of the matrix of PEEK-carbon fiber aromatic polymer composites". In: *SAMPE Q.; (United States)* 17.2 (Oct. 1985), pp. 50–57. URL: https://www.osti.gov/biblio/5054270.

[51] Zhengqi Kou et al. "Optimization of thermal model and prediction of crystallinity during the laser-assisted tape winding process". In: *Journal of Reinforced Plastics and Composites* 40.15-16 (Mar. 2021), pp. 606–618. DOI: 10.1177/0731684421992131. URL: https://doi.org/10.1177/0731684421992131.

[52] Christopher Stokes-Griffin et al. "Thermal modelling of the laser-assisted thermoplastic tape placement process". In: *Journal of Thermoplastic Composite Materials* 28.10 (Nov. 2013), pp. 1445–1462. DOI: 10.1177/0892705713513285. URL: https://doi.org/10.1177/0892705713513285.

[53] Ozan Çelik et al. "The influence of inter-laminar thermal contact resistance on the cooling of material during laser assisted fiber placement". In: *Composites Part A-applied Science and Manufacturing* 145 (June 2021), p. 106367. DOI: 10.1016/j.compositesa.2021.106367. URL: https://doi.org/10.1016/j.compositesa.2021.106367.

[54] Omar Baho et al. "Simulation of laser heating distribution for a thermoplastic composite: effects of AFP head parameters". In: *The International Journal of Advanced Manufacturing Technology* 110.7-8 (Sept. 2020), pp. 2105–2117. DOI: 10.1007/s00170-020-05876-9. URL: https://doi.org/10.1007/s00170-020-05876-9.

[55] Christophe Ageorges et al. "Characteristics of resistance welding of lap shear coupons. Part I: Heat transfer". In: *Composites Part A-applied Science and Manufacturing* 29.8 (Aug. 1998), pp. 899–909. DOI: 10.1016/s1359-835x(98)00022-0. URL: https://doi.org/10.1016/s1359-835x(98)00022-0.

[56] Scott T. Holmes and John W. Gillespie. "Thermal Analysis for Resistance Welding of Large-Scale Thermoplastic Composite Joints". In: *Journal of Reinforced Plastics and Composites* 12.6 (June 1993), pp. 723–736. DOI: 10.1177/073168449301200609. URL: https://doi.org/10.1177/073168449301200609.

[57] Arthur Levy et al. "Modeling of Inter-Layer thermal contact resistance during thermoplastic tape placement". In: *ResearchGate* (Jan. 2012). URL: https://www.researchgate.net/publication/259669209_Modeling_of_Inter-Layer_Thermal_Contact_Resistance_During_Thermoplastic_Tape_Placement.

[58] Thomas Weiler. "Thermal skin effect in laser-assisted tape placement of thermoplastic composites; 1. Auflage". Veröffentlicht auf dem Publikationsserver der RWTH Aachen University; Dissertation, RWTH Aachen University, 2019. Dissertation. Aachen: RWTH Aachen University, 2019, 1 Online–Ressource (X, 203 Seiten) : Illustrationen, Diagramme. ISBN: 978-3-86359-739-9. DOI: 10.18154/RWTH-2019-06638. URL: https://publications.rwth-aachen.de/record/764139.

[59] Els Verdonck. *Differential Scanning Calorimetry (DSC) Practical Training Course*. 2020. URL: https://www.scribd.com/document/659011403/Discovery-DSC-practical-2020-part-1.

[60] TA Instruments. *THERMAL APPLICATIONS NOTE Purge Gas Recommendations for use in Modulated DSC®*. Tech. rep. TN-44. Mar. 1998.

[61] *Toray Cetex® TC1200 PEEK Product Data Sheet*. 2019. URL: https://www.toraytac.com/media/7765d981-1f9f-472d-bf24-69a647412e38/Pr7gdw/TAC/Documents/Data_sheets/Thermoplastic/UD%20tapes,%20prepregs%20and%20laminates/Toray-Cetex-TC1200_PEEK_PDS.pdf.

[62] *HexTow AS4 Product data*. Mar. 2010. URL: https://www.rockwestcomposites.com/media/wysiwyg/AS4_1.pdf.

[63] *HexTow® AS4D Carbon Fiber Product Data Sheet*. 2020. URL: https://www.hexcel.com/user_area/content_media/raw/AS4D_Aerospace_HexTow_DataSheet.pdf.

[64] *Victrex® 150G PEEK Product Data Sheet*. 2017. URL: https://www.victrex.com/-/media/downloads/datasheets/victrextds150g-151g.pdf.

[65] Maciej Giżyński and Barbara Romelczyk-Baishya. "Investigation of carbon fiber–reinforced thermoplastic polymers using thermogravimetric analysis". In: *Journal of Thermoplastic Composite Materials* 34.1 (Apr. 2019), pp. 126–140. DOI: 10.1177/0892705719839450. URL: https://doi.org/10.1177/0892705719839450.

[66] *Suprem® AS4/PA12 Product Data*. 2023. URL: https://www.suprem.ch/materials/.

[67] *Carbolite® ELF11/14 Product Data*. 2023. URL: https://www.carbolite-gero.com/files/12830/laboratory-industrial-ovens-furnaces.pdf%20page%2029.

[68] Moayad N. Khalaf, Dhia A Hassan, and Ali Almowali. "Polymer composite effect of crystallinity and fillers on the heat capacity of polyethylene". In: *ResearchGate* (Jan. 2003). URL: https://www.researchgate.net/publication/313011437_Polymer_Composite_Effect_of_Crystallinity_and_Fillers_on_the_Heat_Capacity_of_Polyethylene.

[69] TATechTips. *Integrating Baselines DSC*. May 2012. URL: https://www.youtube.com/watch?v=tNu9nFtBXNk.

[70] L. Blaine Roger. *Polymer Heats of Fusion*. June 2002. URL: https://www.tainstruments.com/pdf/literature/TN048.pdf.

[71] Manika Varma-Nair and Bernhard Wunderlich. "Heat capacity and other thermodynamic properties of linear macromolecules X. Update of the ATHAS 1980 Data Bank". In: *Journal of Physical and Chemical Reference Data* 20.2 (Mar. 1991), pp. 349–404. DOI: 10.1063/1.555882. URL: https://doi.org/10.1063/1.555882.

[72] Anabela Fernandes. "Accuracy and precision of heat capacity measurements using a heat flux differential scanning calorimeter". In: *www.academia.edu* (Oct. 2021). URL: https://www.academia.edu/57751096/Accuracy_and_precision_of_heat_capacity_measurements_using_a_heat_flux_differential_scanning_calorimeter.

[73] I. Gilmour and J. N. Hay. "Determination of the specific heat of polystyrene by d.s.c." In: *Polymer* 18.3 (Mar. 1977), pp. 281–285. DOI: 10.1016/0032-3861(77)90217-8. URL: https://doi.org/10.1016/0032-3861(77)90217-8.

[74] K. L. Ramakumar, Manoj Saxena, and S.B. Deb. "Experimental Evaluation of Procedures for Heat Capacity Measurement by Differential Scanning Calorimetry". In: *Journal of Thermal Analysis and Calorimetry* 66.2 (Jan. 2001), pp. 387–397. DOI: 10.1023/a:1013126414406. URL: https://doi.org/10.1023/a:1013126414406.

[75] D.J. Blundell. "On the interpretation of multiple melting peaks in poly(ether ether ketone)". In: *Polymer* 28.13 (Dec. 1987), pp. 2248–2251. DOI: 10.1016/0032-3861(87)90382-x. URL: https://doi.org/10.1016/0032-3861(87)90382-x.

[76] Manika Varma-Nair and Bernhard Wunderlich. "Heat capacity and other thermodynamic properties of linear macromolecules X. Update of the ATHAS 1980 Data Bank". In: *Journal of Physical and Chemical Reference Data* 20.2 (Mar. 1991), pp. 349–404. DOI: 10.1063/1.555882. URL: https://doi.org/10.1063/1.555882.

[77] Parina Patel et al. "Mechanism of thermal decomposition of poly(ether ether ketone) (PEEK) from a review of decomposition studies". In: *Polymer Degradation and Stability* 95.5 (May 2010), pp. 709–718. DOI: 10.1016/j.polymdegradstab.2010.01.024. URL: https://doi.org/10.1016/j.polymdegradstab.2010.01.024.

[78] Robert Danley and Peter Caulfield. "DSC Baseline Improvements Obtained by a New Heat Flow Measurement Technique". In: *ResearchGate* (June 2023). URL: https://www.researchgate.net/publication/242610324_DSC_Baseline_Improvements_Obtained_by_a_New_Heat_Flow_Measurement_Technique.

[79] R Danley and J Groh. *Improved DSC Performance Using Tzero Technology*. 2001. URL: https://www.tainstruments.com/pdf/literature/TA271.pdf.

[80] TA Instruments. *TA Instruments User Training*. 2012. URL: https://www.hic.ch.ntu.edu.tw/TA/TA-DSC-TR-PRIN.pdf.

[81] Manika Varma-Nair, Yuan Jin, and Bernhard Wunderlich. "Heat capacities of aliphatic and aromatic polysulphones". In: *Polymer* (Jan. 1992). DOI: 10.1016/0032-3861(92)90812-b. URL: https://doi.org/10.1016/0032-3861(92)90812-b.

A Appendix

A.1 Tzero cell design

As can be seen on Figure 25a, the sample and reference pans sit on the top of two separate thin wall cylinders connected by a constatan body. This novel design provides superior thermal isolation of the heat flows into the sample and reference as well as better reproducibility in terms of pan placement. The sample and reference temperature are measured by area thermocouples on the underside of each platform, while a third temperature sensor in the middle of the body controls the temperature of the furnace. The constatan body is brazed to the chamber enclosure resulting in an isothermal base surface, the furnace is placed underneath the measurement chamber. This arrangement allows for more precise temperature control of the measurement cell due to the closer proximity of the temperature sensor to the sample. Whereas in a conventional heat flux DSC, the chamber temperature is controlled via a thermocuple embedded in the silver furnace.[78] [41] Equation 7 shows the new four term equation for the heat flow calculation.[39]

$$q = -\frac{\Delta T}{R_R} + \Delta T_0\left(\frac{R_R - R_S}{R_R R_s}\right) + (C_R - C_S)\frac{dT_s}{d\tau} - C_r\frac{d\Delta T}{d\tau} \tag{7}$$

,where ΔT is the temperature difference between the sample and reference temperature sensors, R_R is the thermal resistance of the reference side calorimeter, ΔT_0 is the temperature difference between the temperature sensor of the DSC cell (T_0) and the sample temperature sensor (T_S), R_S is the thermal resistance of the sample side calorimeter, C_r and C_S are the reference and sample side calorimeter thermal capacitances respectively, $dT_s/d\tau$ is the heating rate of the sample, lastly $d\Delta T/d\tau$ is the heating rate difference between the sample and reference. The first term of Equation 7 is the same as Equation 2, the second and third term accounts for the thermal imbalances between the sample and reference calorimeters, while the last term compensates for the heating rate difference between reference and sample side. It should be noted that, taking into account the thermal resistances and capacitances of the DSC cell requires a more laborious calibration due to the necessary measurements of these thermal imbalances, instead of assuming their equivalence. However, this approach results in a fundamentally better quantification of the heat flowing into or out of the sample.[79]

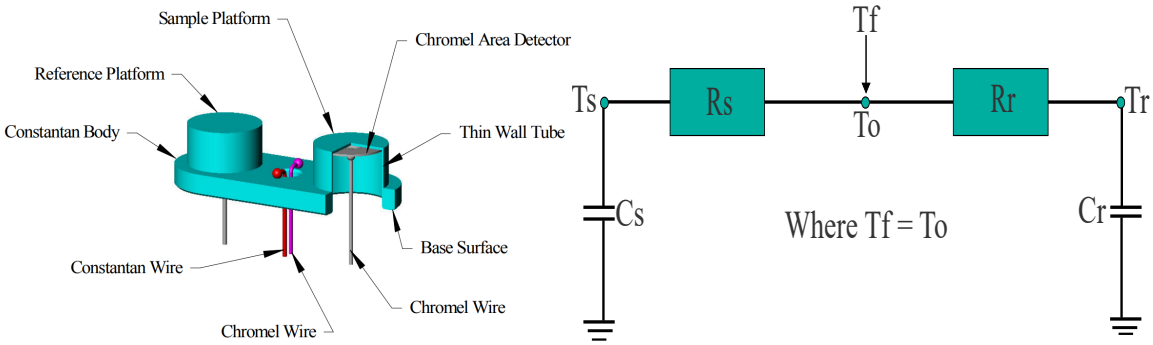

(a) Schematic of Tzero DSC cell [80] (b) Thermal model of the Tzero DSC [41]

Figure 25: Tzero Cell and its thermal circuit

A.2 Literature review

Cecean et. al. [45] measured the temperature dependent specific heat capacity of epoxy and polyester based unidirectional composite materials using glass, carbon and aramid fiber reinforcements. They used a Perkin-Elmer heat-flux DSC for specific heat capacity characterization. Their temperature program consists of three segments, starting with a 6 minute isothermal hold at 20 [°C], then heating up the materials to 250 [°C] with a constant 10[K/min] heating rate and finishing with another isothermal hold for 6 minutes. The experiments were carried out under a constant 50[mL/min] argon purge. The authors followed the three-run method for heat capacity determination, therefore three subsequent DSC runs were completed. The first run, to establish the measurement baseline, is done with two empty crucibles. The second run is completed with a reference material, and finally, the sample is measured. They used alumina as a reference material. The composite samples were fabricated by hand-layup method and were cut into disk shapes to neatly fit the aluminum crucibles. For each composite type - epoxy based glass/carbon/aramid and polyester based glass/carbon/aramid - three samples were tested. In order to ensure a good thermal contact between the samples and the pans, the authors have made an effort to flatten the specimens as good as possible. They noted the difficulty of preparing representative samples for the DSC measurement due to the small size of the pans. They observed a notable discrepancy between the obtained specific heat capacity values of the epoxy/glass and epoxy/carbon fiber composites, despite having the same specific heats of their constituents. They explained this phenomenon with the difference in fiber volume fractions and concluded, that the fibers play a significant role in distributing the thermal energy within the composite materials. They noted a 3.5[%] uncertainty of the specific heat capacity determination with the used instrument over the whole temperature range. However, they have not reported the standard deviation of their obtained results from the three separate sample measurement for the different composite types. Therefore, the dispersion or variability of the obtained specific heat capacities cannot be quantified, hindering the assessment of how scattered or spread out their results are.

Kaloginnakis et. al. [44] have measured the specific heat capacity of cross-ply epoxy based glass and carbon fiber composites using temperature modulated DSC. For this purpose they employed a TA instruments 2920 DSC machine. They tested three samples per material types. The specimens had three layers with a thickness of 0.4 [mm], weighted around 20[mg] and were cut into disk shapes corresponding to the aluminum crucibles used for the measurement. Their temperature program started at -50 [°C] with a 15 minute equilibrium, then samples were heated up to 125 [°C] with a constant 5 [K/min] heating rate. The modulation period was set to 80 [s] with 0.5 [K] modulation. The authors followed the ASTM E1952-98 standard for heat capacity determination. The heat capacity calibration was carried out with a sapphire reference. They have reported remarkably low standard deviations of 2 [%] and 3 [%] for the obtained specific heat capacities of their tested glass and carbon fiber reinforced epoxies respectively. They observed a strong temperature dependence of the specific heats for both materials. The specific heat capacity of carbon/epoxy composite increased by 35 [%] between 20 [°C] and 80 [°C], rising from 0.87 [J/gK] to 1.13 [J/gK]. Meanwhile, the specific

heat capacity of the glass/epoxy composite in the same temperature range showed a smaller, but still significant increase, starting from 0.87 [J/gK] and reaching 1.05 [J/gK], representing a 20 [%] change. With the measured data, the authors used a linear fitting approach to model the temperature dependency of the specific heat capacity for both materials. In order to describe the measured temperature range, they constructed three equations representing the pre-glass transition, glass transition and post-glass transition regions with a high goodness of the fit in all cases. Last but not least, they also noted the difficulty of preparing representative samples for the heat capacity determination due to the small pan sizes.

Forghani [47] in his thesis investigated the influence of modulation parameters, namely the modulation time and modulation temperature, on the accuracy of the resultant specific heat capacity values of CF/PEEK composites using TMDSC (temperature modulated differential scanning calorimetry). Moreover, he has tested the impact of thermal contact resistance on the heat capacity measurements. In all of his experiments the same temperate program was employed, starting with heating up the cell from room temperature (20 [°C]) to 380 [°C] with 3[K/min] heating rate then immediately cooling back down to room temperature with 10[K/min]. This thermal cycle was (heating up and cooling down) was repeated twice. As mentioned above the modulation period and temperature was varied over the experiments. The employed machine was a TA instruments DSC2500 Discovery. The experiments were carried out with prepreg TenCate Cetex® TC1200 CF/PEEK composite materials, without any further processing. The samples weighted between 10-12[mg]. For reference material synthetic sapphire was used. Forghani [47] notes, that following the thermal cycle recommended by the manufactures led to reasonable results with low scatter. However, the specific heat capacity of the all his completed runs still varies between 700 [J/kgK] and 1020 [J/kgK] at 50 [°C] and 1520 [J/kgK] and 1720 [J/kgK] at 360 [°C] showing the 37[%] and 12 [%] deviation respectively. In order to test the impact of thermal contact resistance on the heat capacity measurements as mentioned above, Forghani [47] carried out three subsequent DSC runs with identical thermal cycles using the sapphire reference. Prior to the first run, the sample was manually loaded into the DSC cell. After the completion of the first run, the reference remained in the cell and the second run was carried out. Before the third run, the pan with the sapphire reference was removed from the cell and placed back instantly to carry out the third run. Using this approach Forghani [47] was able to test if any change occurred in the thermal contact resistance between the pan and the DSC cell. From his results, it can be seen that two consecutive run without interfering with the pans were correlating well. However, upon the relocation of a the pan, the resultant specific heat capacity changed significantly, decreasing from 1010 [J/KgK] and 1380 [J/KgK] to 910 [J/KgK] and 1210 [J/KgK] at 50 [°C] and 360 [°C] respectively. He attributed this change solely to the change in thermal contact resistance. It should be noted, that in the first run, the specific heat from the first and second heating ramp deviates notably, therefore some other influencing factors might also play a role, which has not been identified.

In the following study, Kollmannsberger et. al. [48] measured the specific heat capacity of CF/PES composite using Temperature modulated DSC. The experiments were carried out with a TA instruments Q1000 DSC. They have tested 5 samples and reported the average of their results. The specimens were obtained from a three layer laminate processed by a TP-AFP machine. The heating rate was set to 3 [K/min] from 10 [°C] to 420 [°C]. The modulation amplitude was 1 [K] with a modulation period of 100 [s]. They did not entail the method for heat capacity calculation nor the followed standard. From Figure 26 depicted in their study, the scatter of the measured specific heat is about ± 50 [J/kgK] consistently over the measured temperature range. The specific heats of the AS4 fiber and PES matrix shown in Figure 26 were not measured by the authors, but obtained from different sources.[43] [81] With the obtained results, the authors compared the measured specific heat of the CF/PES to the one calculated by the rule of mixtures. They reported a poor correlation from room temperature until the glass transition temperature, however above the glass transition, this discrepancy notably decreased. In their work, they did not elaborate on the cause of this observed trend.

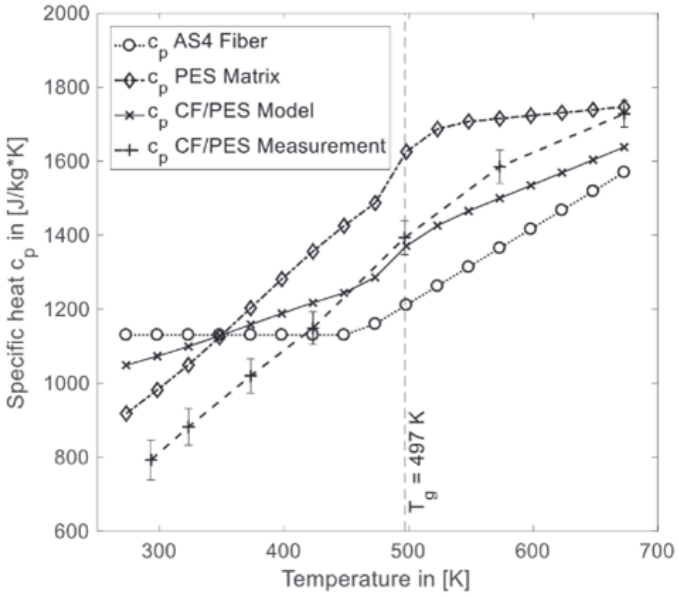

Figure 26: Specific heat capacity of CF/PES obtained by DSC and by ROM [48]

Andrew H. Johnson in his work [43] measured the specific heat capacity of uncured AS4/8852 UD composite material between -40 [°C] and 125 [°C] with a Perking-Elmer Tas 7 DSC machine. He has tested 3 specimens and used their averages for his autoclave process simulation. No mention was found, which standard was followed to obtain the specific heat values nor any information about the samples besides the material. From his data shown in Figure 27, it can be seen that the material exhibits significant scatter in the measured specific heat capacity values across the entire temperature range. However, as the temperature increases, the deviation between the results start to decrease, but remains notable.

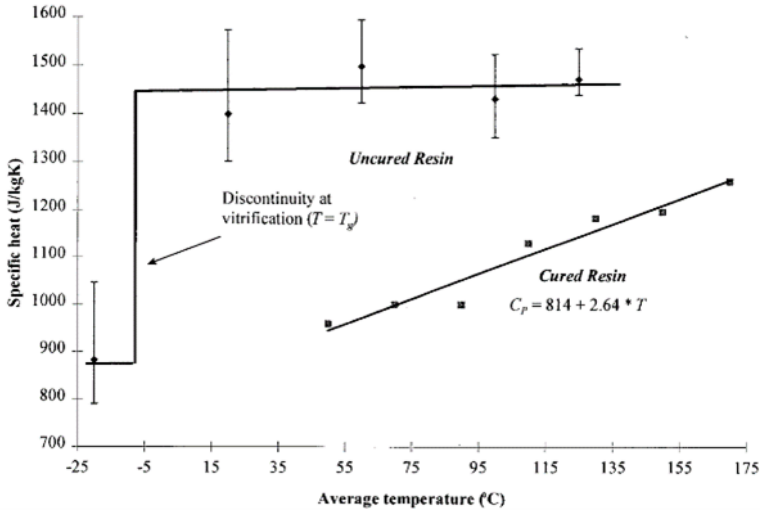

Figure 27: Specific heat capacity of uncured AS4/8852 composite [43]

In his PhD dissertation, Muhammad [46] measured the specific heat capacity of CF/PEEK composite. The unidirectional tape was supplied by Hexcel and the samples were cut from 2 [mm] thick consolidated laminates. The author did not mention the number of tested specimens. The study was carried out with a NETZSCH model LFA 447 Nano-Flash diffusivity machine. No detail was found about the employed temperature program or heating rate. The results were reported at 25 [°C] and at 300 [°C] with values of 0.866 [J/gK] and 1.803 [J/gK] respectively, without the corresponding standard deviations or uncertainties. Lionetto et al. [3] used glass fiber reinforced polypropylene in their study. They obtained the specific heat capacity of their composite by the rule of mixtures. They carried out three dynamic DSC measurement with 10[K/min] between 25 [°C] and 250 [°C] in order to obtain the specific heat capacity of the cured and uncured polypropylene matrix and used the average of their results for further calculation. It is not mentioned from which source they obtained the specific heat of the glass fiber nor the number of the tested samples or the followed standard. With the known fiber volume fraction and the specific heat capacities of the constituents and they have used the rule of mixture to attain the specific heat capacity of the glass fiber/polypropylene composite at room temperature.

A.3 Specific heat capacity results of the the 4ply samples obtained from the first and second heat-up cycle

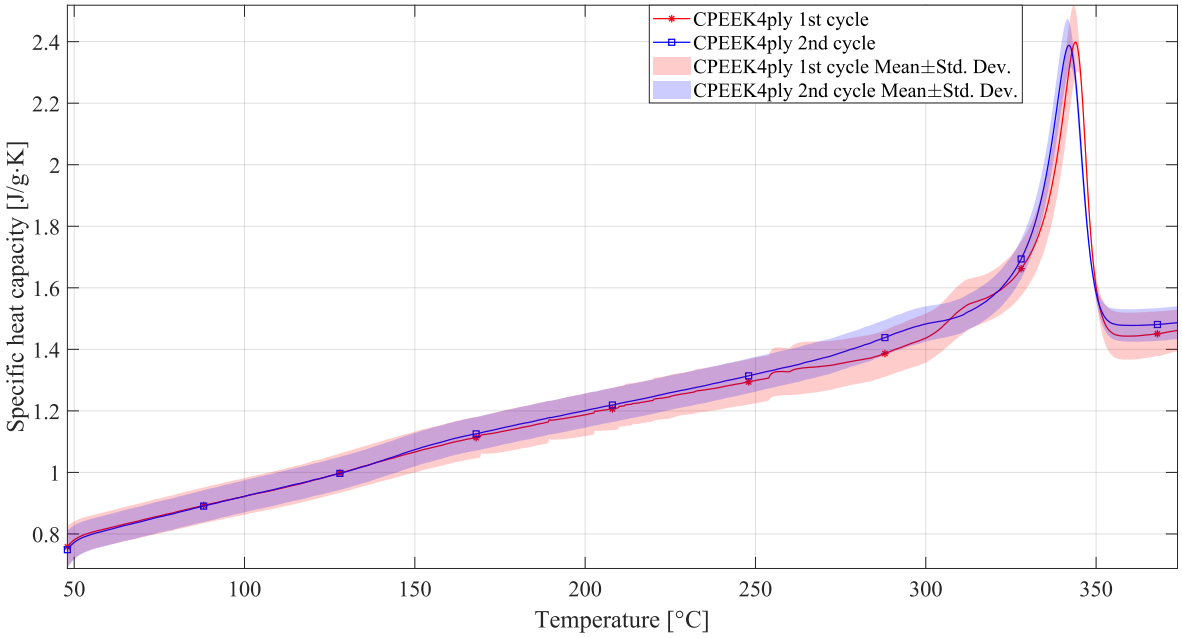

Figure 28: Specific heat capacity results of the the 4ply samples obtained from the first and second heat-up cycle

A.4 Specific heat capacities of the 4ply and 7ply samples with different heating rates

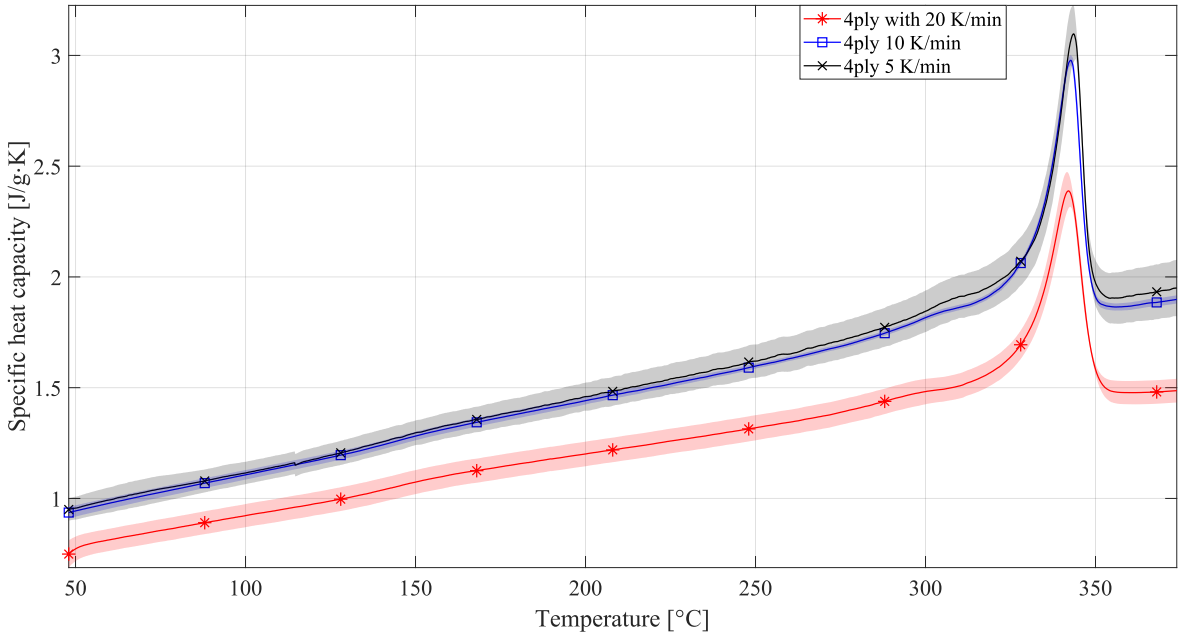

Figure 29: Specific heat capacity of the 4ply samples with heating rates of 20, 10 and 5 K/min

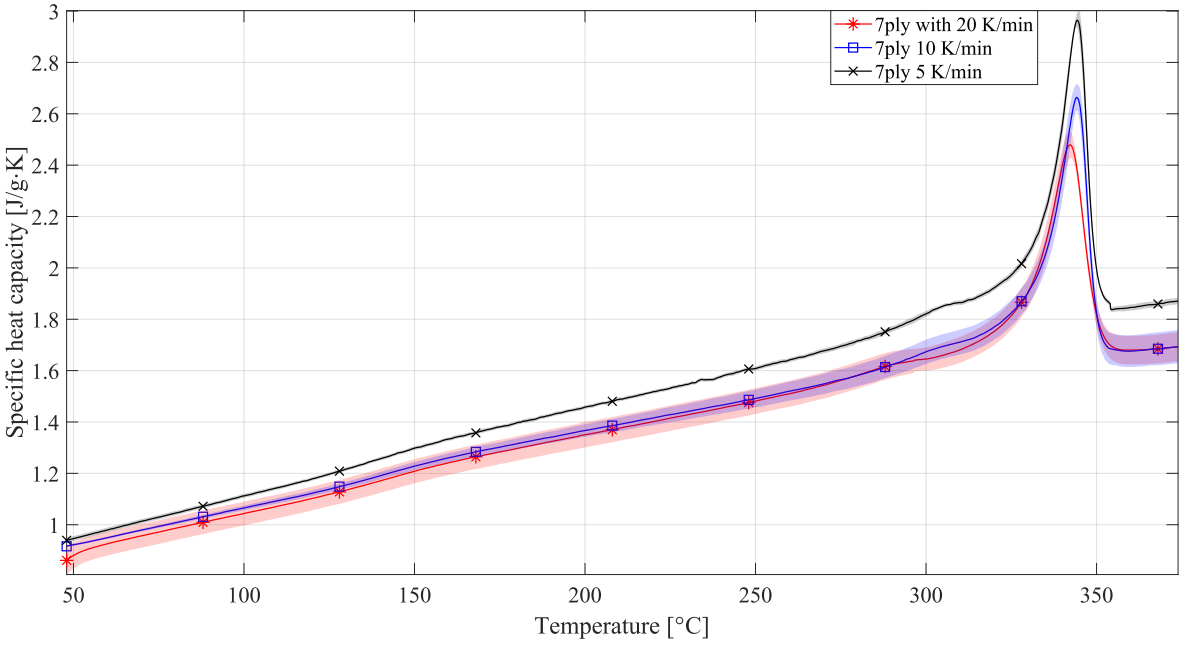

Figure 30: Specific heat capacity of the 7ply samples with heating rates of 20, 10 and 5 K/min

A.5 Specific heat capacities of the neat PEEK samples and dry carbon fibers with different heating rates

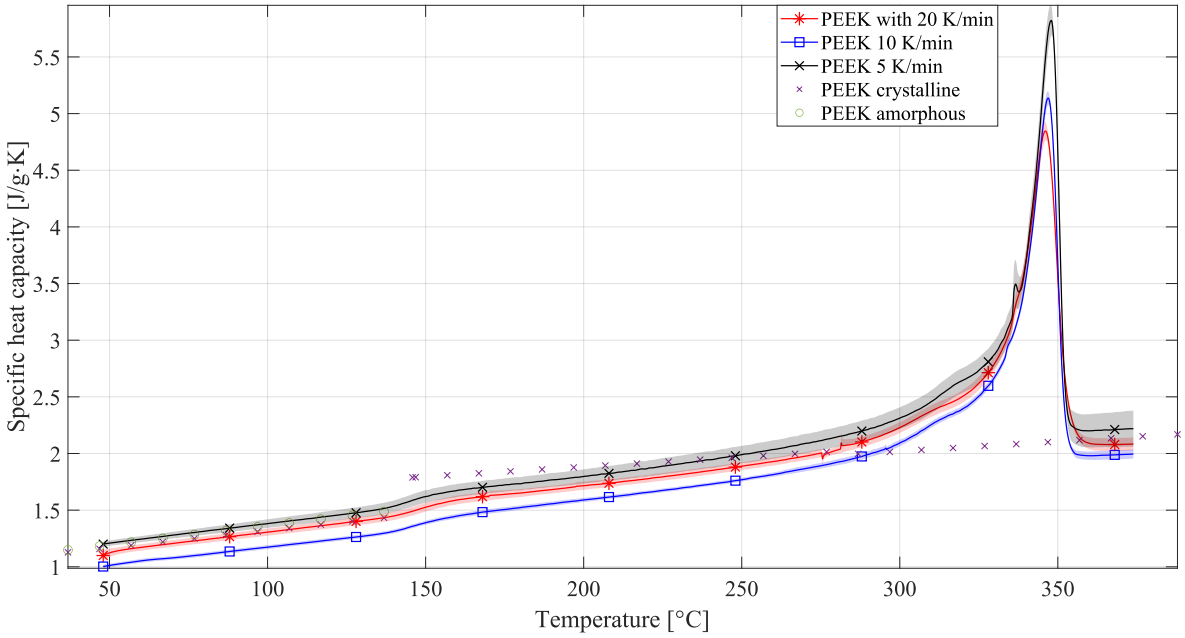

Figure 31: Specific heat capacity of the neat PEEK samples with heating rates of 20, 10 and 5 K/min

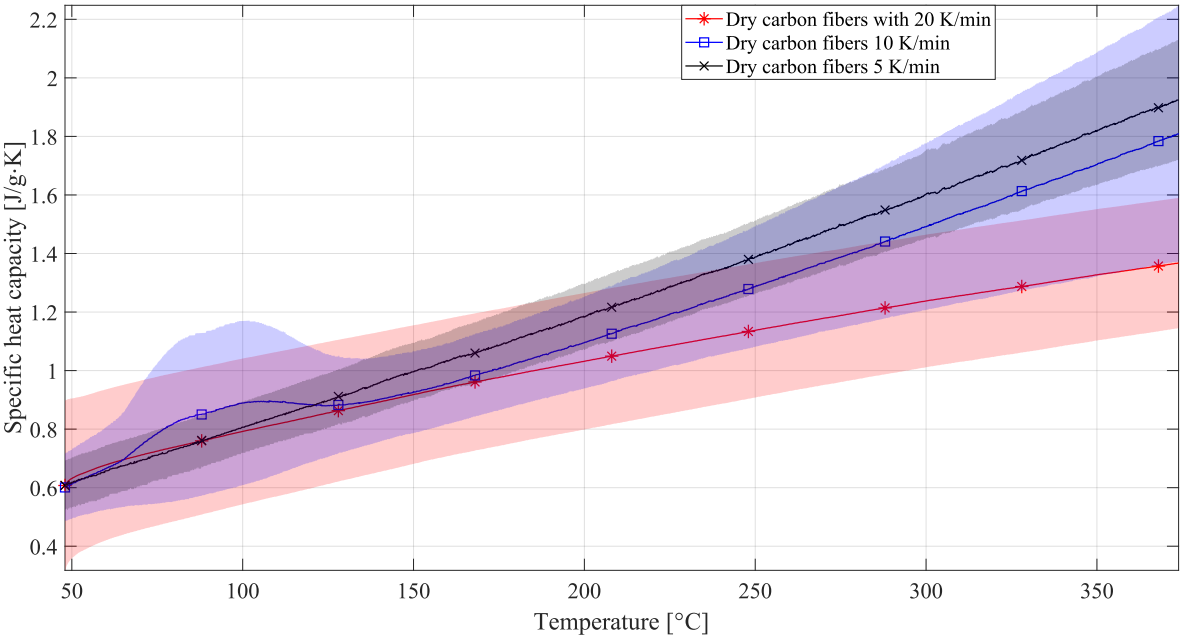

Figure 32: Specific heat capacity of the dry carbon fiber samples with heating rates of 20, 10 and 5 K/min

A.6 Specific heat capacities from the rule of mixtures with different heating rates

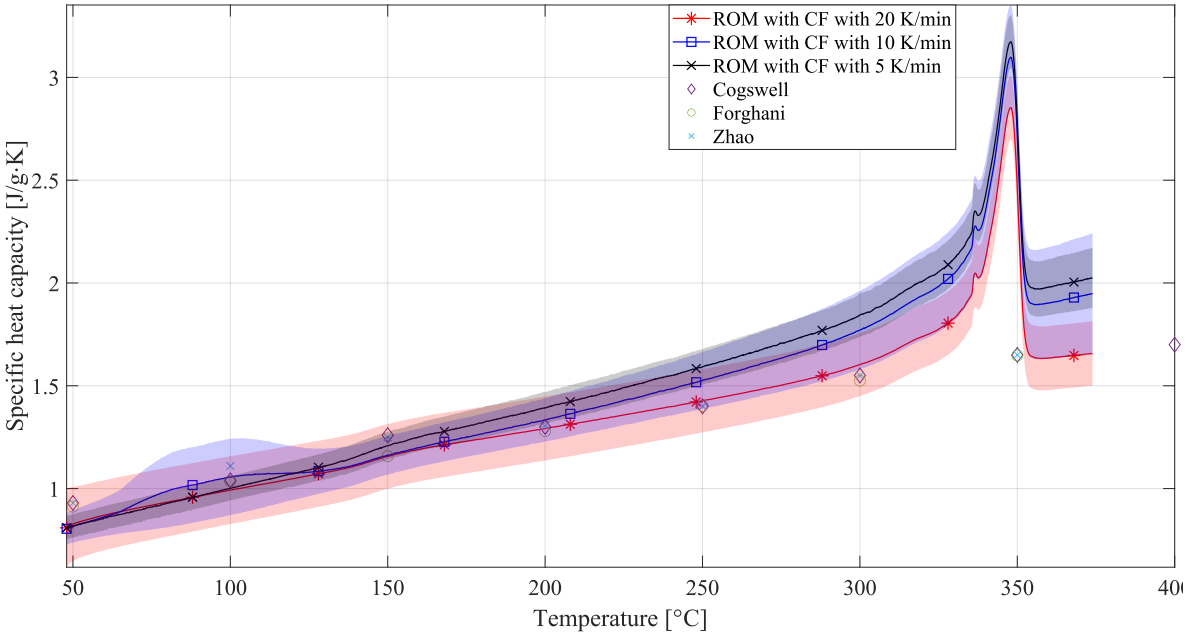

Figure 33: Specific heat capacity from the rule of mixtures with heating rates of 20, 10 and 5 K/min

A.7 Comparison of the 4ply samples with 5 K/min heating rate and the 7ply samples with 5 K/min heating rate with the literature values and their result using the mirrored cooling baselines

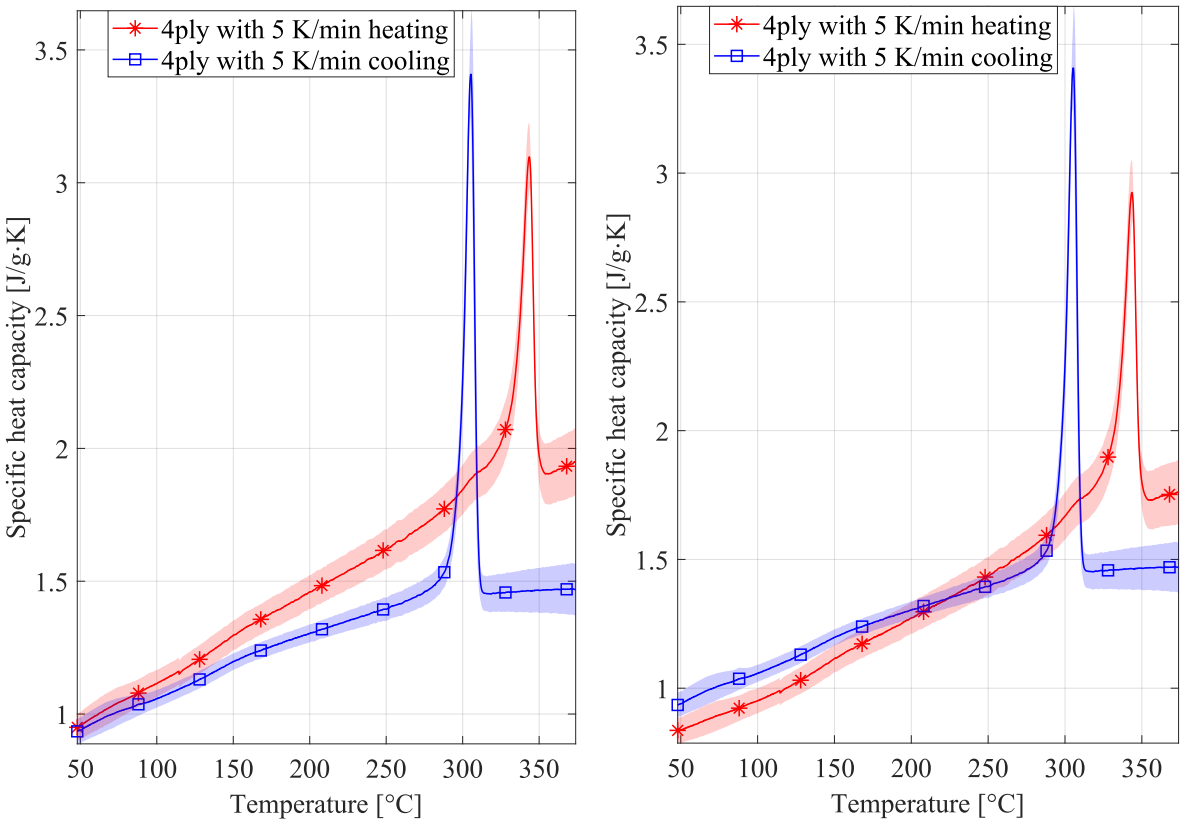

(a) Cp of the 4ply samples with 5 K/min heating rate

(b) Cp of the 4ply samples using mirrored the cooling baseline

Figure 34: Comparison of the measured specific heat capacities of the 4ply samples to literature

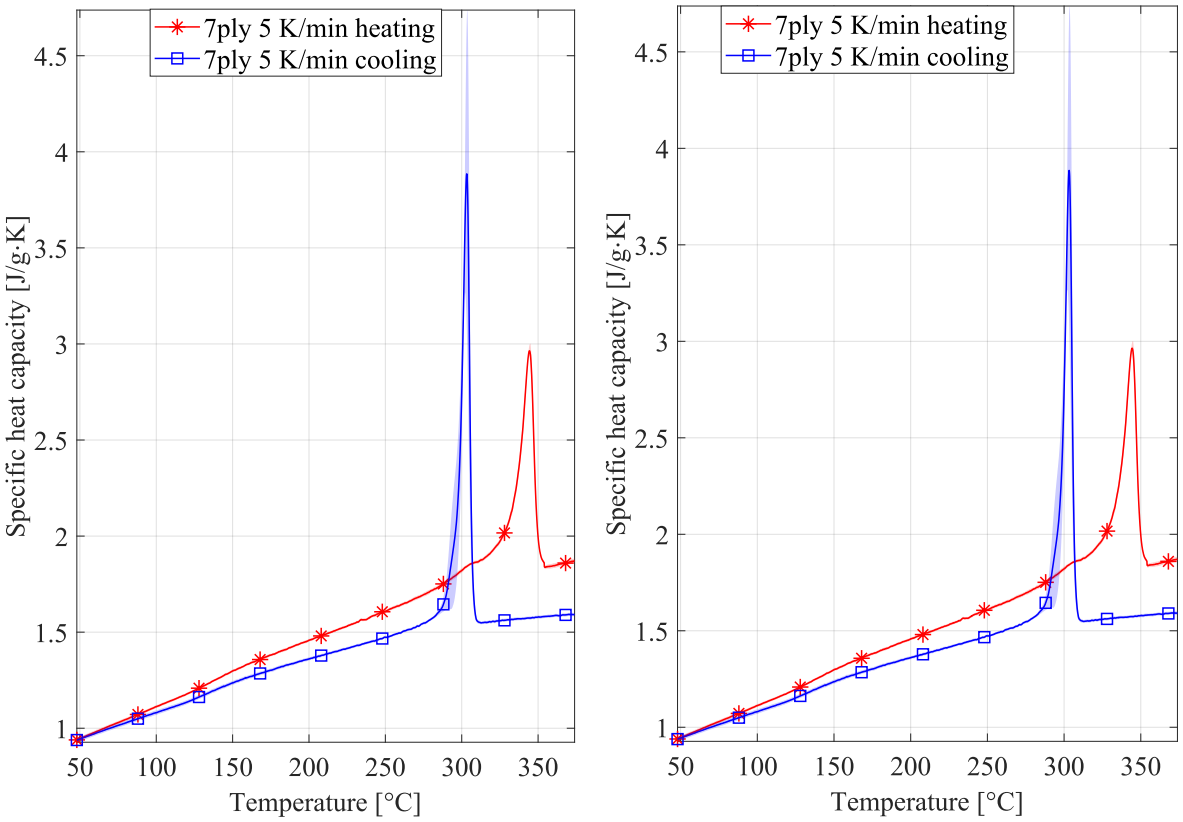

(a) Cp of the 7ply samples with 5 K/min heating rate

(b) Cp of the 7ply samples using mirrored the cooling baseline

Figure 35: Comparison of the measured specific heat capacities of the 7ply samples to literature